



HAL
open science

Data synergy between leaf area index and clumping index Earth Observation products using photon recollision probability theory

Jan Pisek, Henning Buddenbaum, Fernando Camacho, Joachim Hill, Jennifer L.R. Jensen, Holger Lange, Zhili Liu, Arndt Piayda, Yonghua Qu, Olivier Roupsard, et al.

► To cite this version:

Jan Pisek, Henning Buddenbaum, Fernando Camacho, Joachim Hill, Jennifer L.R. Jensen, et al.. Data synergy between leaf area index and clumping index Earth Observation products using photon recollision probability theory. Remote Sensing of Environment, 2018, 215, pp.1-6. 10.1016/j.rse.2018.05.026 . hal-02621001

HAL Id: hal-02621001

<https://hal.inrae.fr/hal-02621001>

Submitted on 16 Sep 2024

HAL is a multi-disciplinary open access archive for the deposit and dissemination of scientific research documents, whether they are published or not. The documents may come from teaching and research institutions in France or abroad, or from public or private research centers.

L'archive ouverte pluridisciplinaire **HAL**, est destinée au dépôt et à la diffusion de documents scientifiques de niveau recherche, publiés ou non, émanant des établissements d'enseignement et de recherche français ou étrangers, des laboratoires publics ou privés.



Distributed under a Creative Commons Attribution - NonCommercial - NoDerivatives 4.0 International License

This document is the accepted manuscript version of the following article:
Pisek, J., Buddenbaum, H., Camacho, F., Hill, J., Jensen, J. L. R., Lange, H.,
... Vuolo, F. (2018). Data synergy between leaf area index and clumping index
Earth Observation products using photon recollision probability theory. Remote
Sensing of Environment, 215, 1-6. <https://doi.org/10.1016/j.rse.2018.05.026>

1 This manuscript version is made available under the CC-BY-NC-ND 4.0 license
<http://creativecommons.org/licenses/by-nc-nd/4.0/>

2

3 **Data synergy between leaf area index and clumping index Earth Observation**
4 **products using photon recollision probability theory**

5

6 Jan Pisek^{1*}, Henning Buddenbaum², Fernando Camacho³, Joachim Hill², Jennifer L.R.

7 Jensen⁴, Holger Lange⁵, Zhili Liu⁶, Arndt Piayda⁷, Yonghua Qu⁸, Olivier Roupsard⁹, Shawn

8 P. Serbin¹⁰, Svein Solberg⁵, Oliver Sonnentag¹¹, Anne Thimonier¹², Francesco Vuolo¹³

9 ¹Tartu Observatory, University of Tartu, 61602 Tõravere, Tartumaa, Estonia

10 ²Environmental Remote Sensing & Geoinformatics, Faculty of Environmental and
11 Regional Sciences, Trier University, D-54286 Trier, Germany

12 ³EOLAB, Parc Científic Universitat de València, c/ Catedràtic José Beltrán, 2. 46980
13 Paterna, Valencia, Spain

14 ⁴Department of Geography, Texas State University San Marcos, TX 7866, USA

15 ⁵Norwegian Institute of Bioeconomy Research, Ås, Akershus, Norway

16 ⁶Center for Ecological Research, Northeast Forestry University, Harbin 150040, China

17 ⁷Thünen Institute of Climate-Smart Agriculture, Bundesallee 65, 38116 Braunschweig,
18 Germany

19 ⁸State Key Laboratory of Remote Sensing Science, Beijing Key Laboratory for Remote
20 Sensing of Environment and Digital Cities, School of Geography, Beijing Normal
21 University, Beijing 100875, China

22 ⁹CIRAD-Persyst, UMR Ecologie Fonctionnelle and Biogéochimie des Sols et
23 Agroécosystèmes, SupAgro-CIRAD-INRA-IRD, Montpellier, France

24 ¹⁰Brookhaven National Laboratory, Environmental & Climate Sciences Department,
25 Upton, NY 11973-5000, USA

26 ¹¹Département de géographie and Centre d'études nordiques, Université de Montréal,
27 Montréal, QC H2V 2B8, Canada

28 ¹²WSL-Swiss Federal Institute for Forest, Snow and Landscape Research, Zürcherstrasse
29 111, 8903 Birmensdorf, Switzerland

30 ¹³Institute of Surveying, Remote Sensing and Land Information, Peter-Jordan-Straße 82
31 1190 Vienna, Austria

32 *Corresponding author. E-mail address: janpisek@gmail.com (J. Pisek)

33

34

35 **Abstract**

36 Clumping index (CI) is a measure of foliage aggregation relative to a random distribution
37 of leaves in space. The CI can help with estimating fractions of sunlit and shaded leaves
38 for a given leaf area index (LAI) value. Both the CI and LAI can be obtained from global
39 Earth Observation data from sensors such as the Moderate Resolution Imaging
40 Spectrometer (MODIS). Here, the **synergy** between a MODIS-based CI and a MODIS LAI
41 product is examined using the theory of spectral invariants, also referred to as photon
42 recollision probability (*p*-theory), along with raw LAI-2000/2200 Plant Canopy Analyzer
43 data from 75 sites distributed across a range of plant functional types. The *p*-theory
44 describes the probability (*p*-value) that a photon, having intercepted an element in the
45 canopy, will recollide with another canopy element rather than escape the canopy. We
46 show that empirically-based CI maps **can be integrated** with the MODIS LAI product. Our
47 results indicate that it is feasible to derive **approximate** *p*-values for any location solely
48 from Earth Observation data. This **approximation** is relevant for future applications of
49 the photon recollision probability concept for global and local monitoring of vegetation
50 using Earth Observation data.

51

52 **Keywords:** Photon recollision probability; Foliage clumping index; Leaf area index; Multi-
53 angle remote sensing

54

55

56 **1. Introduction**

57 Clumping index (CI) is a measure of foliage aggregation relative to a random
58 distribution of leaves in space (Nilson, 1971; Chen and Black, 1992). The CI is an
59 important factor for the correct quantification of true leaf area index (LAI). The CI is also
60 needed for estimating fractions of sunlit and shaded leaves in the canopy (Norman,
61 1982) - an effective way for upscaling from leaf to canopy for modeling vegetation
62 photosynthesis (Bonan et al., 2014; He et al., 2017; Jiang and Ryu, 2016). Global and
63 regional scale CI maps have been generated from various multi-angle sensors (e.g. He et
64 al., 2012; Pisek et al., 2010; 2013a; Wei and Fang, 2016) based on an empirical
65 relationship with the normalized difference between hotspot and darkspot (NDHD)
66 index (Chen et al., 2005). Ryu et al. (2011) suggested that the adequate representation
67 of canopy radiative transfer, important for the simulation of gross primary productivity
68 and evapotranspiration (Baldocchi and Harley, 1995), is possible by integrating CI with
69 incoming solar irradiance and LAI from Moderate Resolution Imaging Spectrometer
70 (MODIS) land and atmosphere products. It should be noted that the MODIS LAI/FPAR
71 product (MOD15A2H) uses internal a set of non-empirical, stochastic equations for the
72 parameterization of foliage clumping (Shabanov et al., 2003). Our objective is to find out
73 if the MODIS LAI product with its non-empirical, stochastic clumping parameterization
74 can be used together with empirically-based CI maps, e.g. for the calculation of
75 sunlit/shaded fractions of LAI.

76 Here, we assess the synergy between a MODIS-based CI (He et al., 2012) and a
77 MODIS LAI product (Yan et al., 2016a,b) using the theory of spectral invariants or 'p-
78 theory' (Knyazikhin et al., 1998) along with raw LAI-2000/2200 Plant Canopy Analyzer

79 (PCA; LI-COR Biosciences, Lincoln, NE, USA) data from 75 sites surveyed across a range
80 of plant functional types (PFTs). The p -theory predicts that the amount of radiation
81 scattered (reflected or transmitted) within a canopy depends only on the wavelength
82 and the spectrally invariant canopy structural parameter p . It can be interpreted as the
83 probability of a photon, having intercepted an element in the canopy, to recollide with
84 another canopy element rather than escape the canopy (Smolander and Stenberg,
85 2005). The parameter p is linked to the foliage clumping (Stenberg et al., 2016).
86 Simulation studies by Möttus et al. (2009) and Smolander and Stenberg (2005) showed
87 the recollision probability is closely related to LAI, with p -LAI relationships varying with
88 the degree of clumping in the spatial distribution of leaf (needle) area. At a fixed LAI, p -
89 value is larger the more aggregated the leaves in a canopy, or the smaller the canopy CI.
90 The p -theory is intuitive and connected to the radiative transfer theory through the
91 eigenvalues of the radiative transfer equation (Knyazikhin et al., 1998). Stenberg et al.
92 (2016) provide an excellent review of the photon recollision probability concept in
93 modelling the radiation regime of canopies.

94

95 **2. Materials and methods**

96 2.1 Method

97 Stenberg (2007) proposed to approximate a photon recollision probability for a
98 canopy (p -value) from the Plant Canopy Analyzer (PCA) as:

$$99 \quad p = 1 - (i_0 / LAI_{true}) \quad (1)$$

100 where p is photon recollision probability, LAI_{true} is true leaf area index, and i_0 is canopy
 101 interceptance (the portion of the incoming radiation (photons) that is intercepted by the
 102 leaves), which can be expressed as:

$$103 \quad i_0 = 1 - t_0 \quad (2)$$

104 where i_0 and t_0 are canopy interceptance and transmittance under diffuse, isotropic
 105 illumination conditions with constant directional intensity (Stenberg, 2007). Both i_0 and
 106 t_0 describe first interactions (with the canopy or the ground) only, and do not include
 107 photons which escape or interact again after being scattered from a leaf or the ground
 108 (Stenberg, pers. comm). Stenberg (2007) and Smolander and Stenberg (2005) further
 109 assume the canopy to have spherical leaf/shoot orientation and to be bounded
 110 underneath by a non-reflecting surface. t_0 is obtained as:

$$111 \quad t_0 = \overline{cgf} \quad (3)$$

112 where \overline{cgf} is the canopy gap fraction at zenith angle θ (averaged over azimuth angle
 113 and horizontal area). Eqs. (1,2) can be combined to give:

$$114 \quad i_0 = 1 - \overline{cgf} \quad (4)$$

115 It should be noted that p as defined by Stenberg (2007) is a canopy structural
 116 characteristic which is independent of the above canopy radiation conditions. The PCA-
 117 based LAI estimate (LAI_{PCA}) is calculated here as the mean of the logarithms of the gap
 118 fraction values with clumping effects partially considered (Ryu et al., 2010):

$$119 \quad LAI_{PCA} = \frac{1}{n} \sum_{i=1}^n \ln \left(\frac{1}{1 - i_0} \right) \quad (5)$$

120 For the coniferous sites, the PCA estimate (LAI_{PCA}) is further converted to true LAI using
121 a shoot-scale grouping correction factor γ_E ($LAI_{true}=LAI_{PCA}*\gamma_E$) before calculating p
122 (Rautiainen et al., 2009).

123 Alternatively, t_0 can be also estimated for an effective zenith angle θ as a
124 function of LAI, mean projection of unit foliage area (G) (Ross, 1981), and clumping
125 index (CI) (Chen et al., 2005):

$$126 \quad t_0(\theta)=\exp[-G(\theta)CI LAI_{true}/\cos\theta] \quad (6)$$

127 Combining Eqs. (1) and (2) with (6), photon recollision probability p can then be
128 calculated with CI and LAI estimated from Earth Observation data as:

$$129 \quad p=1-(1-\exp[-G(\theta)CI LAI_{true}/\cos\theta])/LAI_{true} \quad (7)$$

130 with $G(\theta)=0.5$ and θ set as 57.3° to minimize the uncertainty about leaf angle
131 orientation information (Pisek et al., 2013b) and assuming that t_0 in Eq. (2) for the upper
132 hemisphere can be approximated by $t_0(57.3^\circ)$. Eqs. (4) and (7) provide a simple way to
133 evaluate the synergy of MODIS LAI (Yan et al., 2016a) and CI (He et al., 2012) products
134 with independent PCA estimates. In case of needleleaf forests, Eq. (7) needs to be
135 further modified when used in combination with the MODIS LAI product (LAI_{MODIS}):

$$136 \quad p=1-(1-\exp[-G(\theta) CI \gamma_E LAI_{MODIS}/\cos\theta])/(LAI_{MODIS} \gamma_E) \quad (8)$$

137 as vegetation clumping is not accounted for at the shoot scale in the original MODIS LAI
138 product (Yan et al., 2016b).

139

140 2.2 MODIS LAI data

141 The current version of the MODIS LAI/FPAR product (MOD15A2H) is Collection 6
142 (C6) (Yan et al., 2016a). The main algorithm is based on look-up tables (LUTs) simulated
143 from a three-dimensional radiative transfer (3D RT) model (Knyazikhin et al., 1999;
144 Myneni et al., 2002). The algorithm finds the best LAI and FPAR estimates with biome-
145 specific LUTs using daily land surface Bi-directional Reflectance Factors (BRFs) along with
146 their uncertainties. A back-up empirical method utilizes relationships between the
147 Normalized Difference Vegetation Index and LAI/FPAR to produce lower quality LAI
148 estimates. The LAI value corresponding to the maximum FPAR is selected over the
149 compositing period of four or eight days. Vegetation clumping in the 3D RT is accounted
150 for at plant and canopy scales.

151 The most important improvement in MOD15A2H C6 compared to previous
152 versions is the increase from 1 km to 500 m spatial resolution. In addition, a new version
153 of MODIS surface reflectances (MOD09GA C6) is used to replace the previous 1 km
154 intermediate dataset (MODAGAGG). In C6 the 1 km static land cover input is replaced
155 with new multi-year MODIS land cover product (MCD12Q1) at 500 m resolution.

156 Only MODIS LAI retrievals produced with the main RT algorithm closest to the
157 date of PCA measurements (see Section 2.4) were used in this study.

158

159 2.3 MODIS CI data

160 He et al. (2012) derived a global CI map at 500 m spatial resolution using the red
161 band (620-670 nm) from the MODIS BRDF Model Parameters product (MCD43A1;
162 Schaaf et al., 2002). Since MODIS does not observe near the hotspot and the angular

163 kernels used to construct the MODIS BRDF product do not include the complete hotspot
164 physics and consistently underestimate the hotspot, He et al. (2012) developed an
165 approach to correct the MODIS hotspot magnitude with synchronous co-registered
166 POLDER-3 data. After the MODIS hotspot correction, CI is derived using two coefficients
167 calculated from the second-order polynomial fit of the tabulated relationship between
168 CI and NDHD by Chen et al. (2005). He et al. (2012) assigned a single annual CI value, the
169 median from its noisy seasonal trajectory, to each pixel in the final map. This global CI
170 map is provided using the same pixel grid and projection as the MODIS LAI product
171 (Section 2.2).

172

173 2.4 Plant Canopy Analyzer data

174 Ryu et al. (2010) compiled raw PCA instrument data from 41 sites distributed
175 across six plant functional types ranging from boreal to tropical ecoclimatic zones. PCA
176 data from 34 sites from their synthesis data set were retained after assessing their
177 suitability for our study (e.g. representativeness of the area at the scale of
178 corresponding overlapping 500 m MODIS pixel footprint verified with Google Earth
179 Engine (Gorelick et al., 2017); temporal overlap with MODIS LAI product) (Table 1). In
180 addition to the retained sites from Ryu et al. (2010), PCA measurements from 41
181 additional sites were included in this study. The available raw PCA data were used to
182 approximate p -value at each site using Eq. (4). The corresponding γ_E values for given
183 coniferous species were obtained from literature and are provided in Table 1.

184 Table 1. Characteristics and results for 75 sites with raw PCA measurements. PFT is plant
185 functional type. Lat is latitude (in degrees). Lon is longitude (in degrees). PCA is Plant

186
187

Canopy Analyzer. LAI_{PCA} is LAI estimate from PCA data. p is the photon recollision probability. γ_E is the needle-to-shoot area ratio.

PFT	Country	Site name	Lat	Lon	Species	raw PCA data source	LAI_{PCA}	t_0	p	γ_E
CRO	Austria	Marchfeld_B	48.16N	16.7E	Beet	Vuolo et al. (2016)	2.87	0.095	0.72	
CRO	Austria	Marchfeld_M	48.18N	16.92E	Maize	Vuolo et al. (2016)	3.10	0.089	0.72	
CRO	Austria	Marchfeld_W	48.18N	16.91E	Wheat	Vuolo et al. (2016)	0.55	0.683	0.48	
CRO	China	Heilongjiang	48.13N	126.96E	Corn	Qu et al. (2016)	0.72	0.548	0.42	
CRO	Costa Rica	Aquiaries	9.93N	83.71W	Coffee	Taugordeau et al. (2014)	2.66	0.107	0.70	
CRO	Japan	Nagaoka	37.48N	138.78E	Rice – early planted	Kobayashi (unpublished)	2.72	0.124	0.70	
CRO	Japan	Nagaoka	37.48N	138.78E	Rice – later planted	Kobayashi (unpublished)	2.84	0.111	0.71	
CRO	Spain	Barrax C-3	39.06N	2.09W	Corn	Verger et al. (2009)	0.36	0.746	0.35	
CRO	Spain	Barrax C-2	39.05N	2.09W	Corn	Verger et al. (2009)	0.42	0.715	0.37	
DBF	Estonia	Järvselja	58.29N	27.26E	Silver birch	Kodar et al. (2008)	3.78	0.081	0.76	
DBF	Germany	Hohes Holz	52.08N	11.22E	Beech	Piayda (unpublished)	4.44	0.025	0.79	
DBF	Germany	Merzalben	49.26N	7.8E	Beech, oak	Pueschel et al. (2012)	4.24	0.029	0.77	
DBF	Italy	Ro1	42.41N	11.93E	Oak	Tedeschi et al. (2006)	3.70	0.052	0.75	
DBF	Italy	Ro2	42.39N	11.92E	Oak	Tedeschi et al. (2006)	4.57	0.028	0.79	
DBF	Japan	Takayama	36.14N	137.42E	Mongolian oak	Nasahara et al. (2008)	3.66	0.045	0.74	
DBF	Korea	Gwangneung	37.76N	127.15E	Oak	Kwon (unpublished)	4.57	0.018	0.79	
DBF	Switzerland	Bettlachstock	47.23N	7.41E	Beech	Thimonier et al. (2010)	4.53	0.02	0.79	
DBF	Switzerland	Isonne	46.13N	9.01E	Beech	Thimonier et al. (2010)	3.81	0.035	0.76	
DBF	Switzerland	Lausanne	46.58N	6.66E	Beech	Thimonier et al. (2010)	5.45	0.012	0.82	
DBF	Switzerland	Neunkirch	47.68N	8.53E	Beech	Thimonier et al. (2010)	3.76	0.04	0.75	
DBF	Switzerland	Schänis	47.16N	9.06E	Beech	Thimonier et al. (2010)	4.07	0.03	0.76	
DBF	Switzerland	Novaggio	46.01N	8.83E	Oak	Thimonier et al. (2010)	3.21	0.059	0.72	
DBF	Switzerland	Jussy	46.23N	6.28E	Oak, hornbeam	Thimonier et al. (2010)	4.12	0.031	0.78	
DBF	USA	Chestnut	35.93N	84.45W	Chestnut	Heuer (unpublished)	3.53	0.052	0.73	
DBF	USA	Harvard	42.53N	72.17W	Oak	Urbanski et al. (2007)	4.69	0.022	0.79	
DBF	USA	Coweeta	35.05N	83.45W	Oak-hickory	Hwang et al. (2009)	5.51	0.03	0.83	
EBF	France	Puechabon	43.74N	3.6E	Oak	Rambal et al. (2003)	3.06	0.081	0.70	
EBF	Portugal	Coruche	39.13N	8.33W	Oak	Piayda et al. (2015)	0.73	0.559	0.49	
EBF	Thailand	Kog-Ma	18.8N	98.9E	Lithocarpus	Tanaka et al. (2008)	3.65	0.048	0.74	
ENF	Canada	Scotty Creek	61.31N	121.3W	Black spruce	Sonnentag (unpublished)	0.83	0.514	0.75	1.36
ENF	Canada	Thompson_1850	55.87N	98.47W	Black spruce	Serbin et al. (2009)	2.28	0.206	0.73	1.36
ENF	Canada	Thompson_1930	55.89N	98.51W	Black spruce	Serbin et al. (2009)	2.07	0.214	0.63	1.36
ENF	Canada	Campbell river	49.51N	124.9W	Douglas fir - young	Chen et al. (2006)	2.75	0.108	0.82	1.66
ENF	Estonia	Järvselja	58.3N	27.24E	Norway spruce	Kodar et al. (2008)	3.12	0.095	0.82	1.42
ENF	Estonia	Järvselja	58.3N	27.26E	Scots pine	Kodar et al. (2008)	2.51	0.156	0.80	1.7
ENF	Korea	Gwangneung	37.76N	127.16E	Korean pine	Kwon (unpublished)	4.44	0.021	0.76	1.21
ENF	Norway	Østmarka_1	59.81N	11.0E	Norway spruce	Solberg et al. (2009)	2.17	0.216	0.70	1.42
ENF	Norway	Østmarka_2	59.81N	10.99E	Norway spruce	Solberg et al. (2009)	1.17	0.488	0.87	1.42
ENF	Norway	Østmarka_3	59.82N	11.0E	Norway spruce	Solberg et al. (2009)	5.17	0.021	0.81	1.42
ENF	Norway	Østmarka_5	59.82N	11.02E	Norway spruce	Solberg et al. (2009)	3.26	0.09	0.81	1.42
ENF	Norway	Østmarka_6	59.82N	11.02E	Norway spruce	Solberg et al. (2009)	3.28	0.085	0.84	1.42
ENF	Norway	Østmarka_7	59.81N	11.02E	Norway spruce	Solberg et al. (2009)	4.07	0.05	0.80	1.42
ENF	Norway	Østmarka_8	59.83N	11.03E	Norway spruce	Solberg et al. (2009)	3.11	0.096	0.79	1.42
ENF	Norway	Østmarka_9	59.83N	11.01E	Norway spruce	Solberg et al. (2009)	2.88	0.117	0.80	1.42
ENF	Norway	Østmarka_6_2003	59.82N	11.02E	Norway spruce	Solberg et al. (2009)	3.15	0.104	0.87	1.42
ENF	Norway	Østmarka_3_2003	59.82N	11.0E	Norway spruce	Solberg et al. (2009)	5.27	0.019	0.68	1.42
ENF	Norway	Østmarka_2_2003	59.81N	10.99E	Norway spruce	Solberg et al. (2009)	0.95	0.561	0.78	1.42
ENF	Norway	Østmarka_1_2003	59.81N	11.0E	Norway spruce	Solberg et al. (2009)	2.13	0.219	0.75	1.42
ENF	Switzerland	Alptal	47.05N	8.71E	Norway spruce	Thimonier et al. (2010)	2.73	0.1	0.77	1.42
ENF	Switzerland	Chironico	46.45N	8.81E	Norway spruce	Thimonier et al. (2010)	2.60	0.109	0.72	1.42
ENF	Switzerland	Lens	46.26N	7.43E	Scots pine	Thimonier et al. (2010)	2.09	0.164	0.67	1.7
ENF	Switzerland	Visp	46.3N	7.86E	Scots pine	Thimonier et al. (2010)	1.58	0.248	0.78	1.7
ENF	Switzerland	Vordemwald	47.28N	7.88E	Silver fir	Thimonier et al. (2010)	3.64	0.05	0.79	1.91
ENF	USA	US-NC2	35.48N	76.4W	Loblolly pine	Noormets et al. (2009)	4.23	0.034	0.87	1.21
ENF	USA	Howland	45.21N	68.74W	Red spruce	Richardson (unpublished)	1.94	0.2	0.81	1.6
ENF	USA	SJ57	47.13N	116.18W	Cedar, spruce, larch, pine	Jensen et al. (2011)	2.18	0.175	0.65	1.01
ENF	USA	527	46.22N	116.79W	Fir, pine, spruce, larch	Jensen et al. (2011)	1.94	0.189	0.59	1.01

GRA	Canada	Sandhill	53.79N	104.62W	Sedges	Sonnentag et al. (2010)	1.10	0.459	0.54
GRA	USA	Vaira	38.41N	120.95W	Annual grass	Ryu et al. (2010)	0.99	0.416	0.53
GRA	USA	Sherman	38.04N	121.75W	Invasive weed	Sonnentag (unpublished)	0.61	0.641	0.48
MF	Canada	Timins	48.21N	82.15W	Aspen, spruce, birch, fir	Chen et al. (2006)	3.50	0.068	0.80 1.36
MF	Canada	Thompson_1964	55.91N	98.38W	Spruce, pine, aspen, willow	Serbin et al. (2009)	1.55	0.305	0.65 1.36
MF	Canada	Thompson_1981	55.85N	98.85W	Willow, jack pine, aspen	Serbin et al. (2009)	1.35	0.352	0.62 1.36
MF	Canada	Thompson_1989_1	55.90N	98.95W	Willow, jack pine, aspen	Serbin et al. (2009)	0.91	0.489	0.58 1.36
MF	Canada	Thompson_1989_2	55.91N	98.97W	Willow, jack pine, aspen	Serbin et al. (2009)	0.91	0.489	0.58 1.36
MF	Canada	Thompson_1994	56.16N	96.71W	Willow, jack pine, aspen	Serbin et al. (2009)	0.68	0.578	0.53 1.36
MF	China	SB	47.19N	128.87E	Birch, larch, pine	Liu et al. (2016)	2.32	0.179	0.74 1.08
MF	China	SC	47.19N	128.89E	Pine, birch, beech, elm	Liu et al. (2016)	3.60	0.053	0.80 1.28
MF	China	KP	47.18N	128.88E	Pine, birch, larch	Liu et al. (2016)	3.23	0.086	0.79 1.46
MF	China	BK	47.18N	128.9E	Pine, birch, maple, tilia	Liu et al. (2016)	3.62	0.054	0.80 1.41
MF	Estonia	Järvselja	58.29N	27.25E	Birch, spruce	Kodar et al. (2008)	3.59	0.06	0.81 1.42
MF	USA	WPA	47.63N	122.29W	Fir, maple, cedar, hemlock	Richardson et al. (2009)	2.91	0.082	0.68 1.36
OSH	Canada	Mer Bleue	45.4N	75.5W	Shrub (peatland)	Talbot et al. (2014)	2.69	0.104	0.68
OSH	Canada	Thompson_2003	55.9N	98.18W	Wild rose, fireweed	Serbin et al. (2009)	0.48	0.671	0.41
WSA	USA	Tonzi	38.43N	120.97W	Blue oak	Ryu et al. (2010)	0.68	0.583	0.47

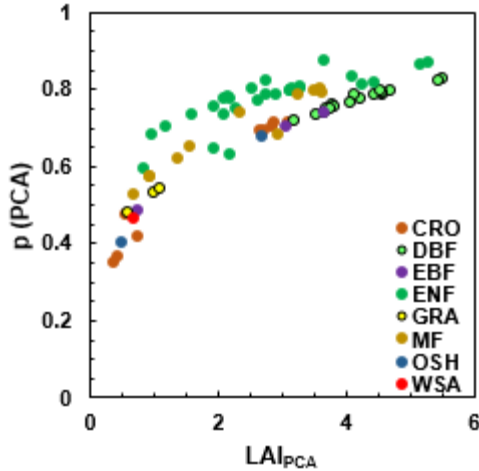
CRO: crop, DBF: deciduous broadleaf forest, EBF: evergreen broadleaf forest, ENF: evergreen needleleaf forest, GRA: grass, MF: mixed forest, OSH: open shrubland, WSA: woody savanna.

188
189
190
191

3. Results and Discussion

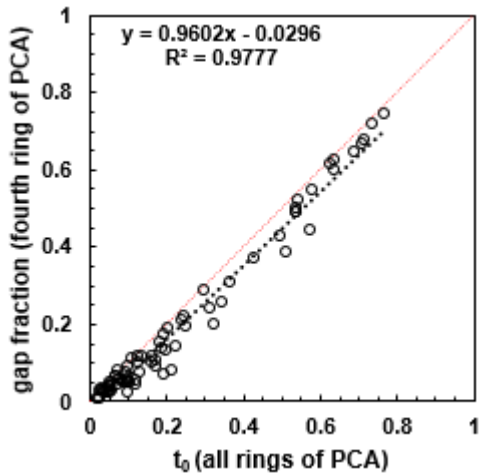
192
193
194
195
196
197
198
199
200

The relationship between LAI and photon recollision probability p approximated with PCA data using Eq. (4) is shown in Fig. 1. The nature of the p -LAI_{PCA} relationship is different between evergreen needleleaf (ENF) and other PFTs due to the inclusion of the shoot-scale correction factor (Chen, 1996). Compared to Rautiainen et al. (2009), the p -values representing needleleaf stands with greater variety of tree species were more dispersed. Our results support the notion by Rautiainen et al. (2009) that establishing species-specific p -LAI_{PCA} functions would require further research on the role of shoot-scale (shoot level) clumping and its documented variability between species (e.g. Chen et al., 2006; Stenberg et al., 1999; 2001) on photon recollision probability.



201

202 | **Fig. 1.** Relationship between Plant Canopy Analyzer (PCA)-derived leaf area index
 203 (LAI_{PCA}) and approximated photon recollision probability p . The abbreviations used in
 204 the figure legend are explained in the caption of Table 1.
 205



206

207 | **Fig. 2.** Comparison between the transmittance (t_0 ; Eq. (3)) and gap fraction from the
 208 fourth ring of Plant Canopy Analyzer (PCA) data.

209

210 Eq. (7) assumes that t_0 in Eq. (3) for the upper hemisphere can be approximated

211 by $t_0(57.3^\circ)$. A regression between the gap fraction from the fourth ring (47–58° from

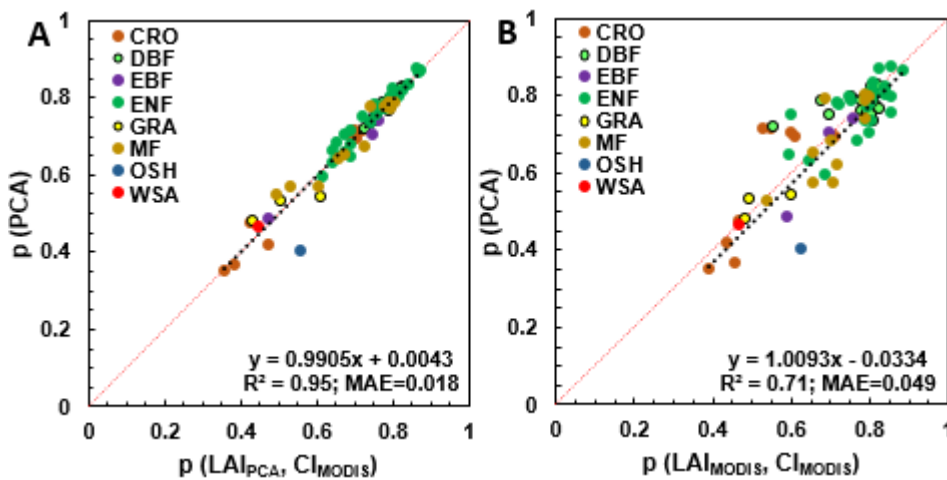
212 zenith) and t_0 obtained from all five rings (Eq. (3)) for all sites is shown in Fig. 2. The tight

213 linear relationship close to the 1:1 line indicates that this ring alone (or 57.3° as its

214 representative) is indeed a reasonable approximation for t_0 of the upper hemisphere,

215 while simultaneously reducing the uncertainty introduced through an assumed leaf
 216 inclination angle distribution. It should be noted that previous research by Leblanc and
 217 Chen (2001) also found that the fourth ring itself provides a good approximation of
 218 LAI_{PCA} under both direct and diffuse light conditions.

219 Fig. 3A shows a strong linear relationship ($R^2=0.95$; Mean Absolute Error (MAE)=
 220 0.018; intercept 0.0043) between the p -values derived from Eqs. (4) and (7)



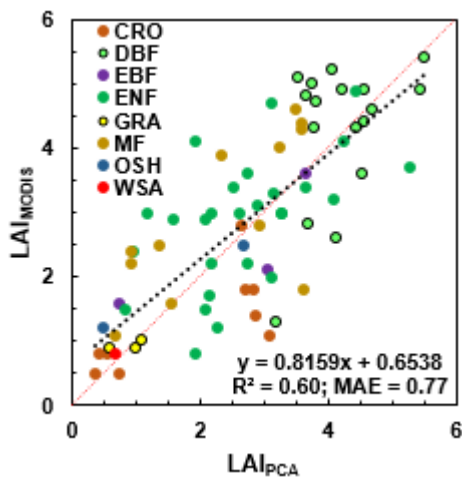
221

222 | **Fig. 3.** Relationships between photon recollision probabilities p derived with Eqs. (4) and
 223 (7) using Plant Canopy Analyzer (PCA) data (A) and MODIS LAI C6 product (B) as LAI
 224 input into Eq. (7).

225

226 using the PCA and γ_E data from Table 1 as the source of information about LAI, and CI
 227 values retrieved from He et al. (2012). Fig. 3A confirms the agreement between the two
 228 approaches (Eqs. (4) and (7)) to obtain p -value. The observed variation stems mainly
 229 from the uncertainty in G-function, CI values and approximation of $t_0(57.3^\circ)$ to t_0 of the
 230 upper hemisphere (Fig. 2). The clumping may change with season (Sprintsin et al., 2011;
 231 Pisek et al., 2015; Lang et al., 2017), while He et al. (2012) provide only the seasonal
 232 trajectory median value.

233 The linear relationship close to the 1:1 line (slope 1.0093; intercept -0.034)
 234 between the p -values derived from PCA and MODIS-only data (Fig. 3B) suggests a
 235 general compatibility of MODIS LAI and CI maps by He et al. (2012). Our results supports
 236 that a) the MODIS algorithm indeed uses the recollision probability to account for
 237 clumping, and b) the approach integrating the empirically based CI information with
 238 MODIS LAI suggested by Ryu et al. (2011) appears to be feasible. The difference
 239 between Figs. 3A and 3B is the inclusion of the MODIS LAI product in the latter one.
 240 Since the clumping in MODIS LAI is accounted for at the plant and canopy scales only,
 241 knowledge about the shoot-scale grouping correction factor γ_E is needed to retrieve the
 242 non-underestimated p -values in case of needleleaf forests.
 243



244
 245 | **Fig. 4.** Relationship between Plant Canopy Analyzer (PCA)-derived leaf area index
 246 (LAI_{PCA}) and MODIS LAI C6 product (LAI_{MODIS}). Both PCA and MODIS LAI data are not
 247 corrected for the shoot-scale grouping correction factor γ_E .

248
 249 Fig. 4 shows the scatterplot between LAI estimates from PCA and MODIS LAI C6
 250 product. The increase in mean absolute error in Fig. 3B (MAE=0.049) compared to Fig.
 251 3A (MAE=0.018) is linked to the different estimates and sources of LAI information for

252 Eq. (4) (PCA) and Eqs. (7) and (8) (MODIS LAI) as illustrated in Fig. 4. Furthermore, Fig. 1
253 shows that accurate LAI information for photon recollision probability estimation is
254 particularly critical at lower LAI values. Since reflectance values are not saturated within
255 LAI range of 0-2, LAI algorithms perform well within this domain (Yan et al., 2016b) and
256 should be able to provide high quality input data. Importantly, it should be verified if the
257 LAI input indeed corresponds to true LAI.

258 Our findings illustrate that it might be possible to obtain approximate p -values
259 for any location solely from Earth Observation data, given availability of high quality LAI
260 retrievals. In the future, the relationship could be possibly strengthened by further
261 improved CI retrieval algorithms from Earth Observation data (e.g. Wei and Fang, 2016),
262 by accounting for seasonal variation of clumping (He et al., 2016) and by knowing site
263 specific G-function values (Raabe et al., 2015). It is envisioned that our findings provide a
264 stimulus for future applications of the photon recollision probability concept for global
265 and local monitoring of vegetation using Earth Observation data (Stenberg et al., 2016).

266

267 **4. Conclusion**

268 Our results indicate that the integration of a MODIS LAI product with empirically-
269 based CI maps is feasible. Their synergy was assessed using the p -theory along with raw
270 LAI-2000/2200 Plant Canopy Analyzer data gathered across a wide range of plant
271 functional types. Importantly, for the first time it is shown that it might be possible to
272 obtain approximate p -values for any location solely from Earth Observation data. This
273 approximation is relevant for future applications of photon recollision probability

274 concept for global and local monitoring of vegetation using Earth Observation data
275 (Stenberg et al., 2016).

276

277 **Acknowledgements**

278 JP was supported by Estonian Research Council Grant PUT1355 and Mobilitas Pluss
279 MOBERC11. The global clumping index map by He et al. (2012) is available for download
280 through the following link:

281 <https://www.researchgate.net/publication/314151326> Global Clumping Index Map.

282 The MODIS LAI C6 data have been accessed through Google Earth Engine. Dr. Youngryel
283 Ryu kindly shared his compilation of raw PCA data. Original providers of the raw PCA
284 data to Dr. Ryu are appreciated: Drs. Jing Ming Chen, Michael Gavazzi, Mark Heuer,
285 Taehee Hwang, Joon Kim, Soo-Hyung Kim, Hideki Kobayashi, John Kochendorfer,
286 Hyojung Kwon, Beverly Law, Craig Macfarlane, Francesco Mazzenga, Mark Mesarch,
287 William Munger, Kenlo Nishida Nasahara, Asko Noormets, Jean-Marc Ourcival, Dario
288 Papale, Serge Rambal, Andrew Richardson, Julie Talbot, Shashi Verma, and Leland
289 Werden. Drs. Martin Béland, Yuri Knyazikhin, Philip Lewis and Pauline Stenberg provided
290 valuable input and comments on the concept provided in this study. Authors wish to
291 thank three anonymous reviewers for constructive comments on the manuscript.

292

293 **References**

294 Baldocchi, D.D., Harley, P.C., 1995. Scaling carbon dioxide and water vapour exchange from leaf to canopy
295 in a deciduous forest. II. Model testing and application. *Plant, Cell & Environment* 18, 1157–1173.

296 Bonan, G. B., Williams, M., Fisher, R. A., & Oleson, K. W. (2014). Modeling stomatal conductance in the
297 earth system: linking leaf water-use efficiency and water transport along the soil-plant-atmosphere
298 continuum. *Geoscientific Model Development*, 7, 2193-2222. doi:10.5194/gmd-7-2193-2014.

299 Burba, G.G., Verma, S.B., 2005. Seasonal and interannual variability in evapotranspiration of native
300 tallgrass prairie and cultivated wheat ecosystems. *Agricultural and Forest Meteorology* 135 (1-4),
301 190-201.

302 Chen, J.M., 1996. Optically-based methods for measuring seasonal variation of leaf area index in boreal
303 conifer stands. *Agricultural and Forest Meteorology* 80, 135-163.

304 Chen, J.M., Black, T.A., 1992. Foliage area and architecture of plant canopies from sunfleck size
305 distributions. *Agricultural and Forest Meteorology* 60, 249-266.

306 Chen, J.M., Menges, C.H., Leblanc, S.G., 2005. Global mapping of foliage clumping index using multi-
307 angular satellite data. *Remote Sensing of Environment* 97, 447-457.

308 Chen, J.M., Govind, A., Sonnentag, O., Zhang, Y.Q., Barr, A., Amiro, B., 2006. Leaf area index
309 measurements at Fluxnet-Canada forest sites. *Agricultural and Forest Meteorology* 140, 257-268.

310 Gorelick, N., Hancher, M., Dixon, M., Ilyushchenko, S., Thau, D., Moore, R., 2017. Google earth engine:
311 Planetary-scale geospatial analysis for everyone. *Remote Sensing of Environment* 202, 18-27.

312 He, L., Chen, J.M., Pisek, J., Schaaf, C.B., Strahler, A.H., 2012. Global clumping index map derived from the
313 MODIS BRDF product. *Remote Sensing of Environment* 119, 118-130.

314 He, L., Liu, J., Chen, J.M., Croft, H., Wang, R., Sprintsin, M., Zheng, T., Ryu, Y., Pisek, J., Gonsamo, A., Deng,
315 F., and Zhang, Y. (2016). Inter- and intra-annual variations of clumping index derived from the MODIS
316 BRDF product. *International Journal of Applied Earth Observation and Geoinformation*, 44, 53-60.

317 He, L., Chen, J. M., Croft, H., Gonsamo, A., Luo, X., Liu, J., . . . Liu, Y. (2017). Nitrogen Availability Dampens
318 the Positive Impacts of CO₂ Fertilization on Terrestrial Ecosystem Carbon and Water Cycles.
319 *Geophysical Research Letters*, n/a-n/a. doi:10.1002/2017GL075981.

320 Hwang, T., Band, L.E., Hales, T.C., 2009. Ecosystem processes at the watershed scale: extending optimality
321 theory from plot to catchment. *Water Resources Research* 45 (W11425),
322 doi:10.1029/2009WR007775.

323 Jensen, J. L. R., Humes, K. S., Vierling, L. A., & Hudak, A. T., 2008. Discrete return lidar-based prediction of
324 leaf area index in two conifer forests. *Remote Sensing of Environment* 112, 3947–3957.

325 Jiang, C., & Ryu, Y. (2016). Multi-scale evaluation of global gross primary productivity and
326 evapotranspiration products derived from Breathing Earth System Simulator (BESS). *Remote Sensing*
327 *of Environment*, 186, 528-547.

328 Knyazikhin, Y.; Glassy, J.; Privette, J.L.; Tian, Y.; Lotsch, A.; Zhang, Y.; Wang, Y.; Morisette, J.T.; Votava, P.;
329 Myneni, R.B., 1999. MODIS Leaf Area Index (LAI) and Fraction of Photosynthetically Active Radiation
330 Absorbed by Vegetation (FPAR) Product (MOD15) Algorithm Theoretical Basis Document; Theoretical
331 Basis Document; NASA Goddard Space Flight Center: Greenbelt, MD, USA, 1999; p. 20771.

332 Knyazikhin, Y., Martonchik, J., Myneni, R., Diner, D., Running, S., 1998. Synergistic algorithm for estimating
333 vegetation canopy leaf area index and fraction of absorbed photosynthetically active radiation from
334 MODIS and MISR data. *Journal of Geophysical Research* D103(32), 257–32 276.

335 Kodar, A., Kutsar, R., Lang, M., Lukk, T., Nilson, T., 2008. Leaf area indices of forest canopies from optical
336 measurements. *Baltic Forestry* 14 (2), 185–194.

337 Lang, M., Nilson, T., Kuusk, A., Pisek, J., Korhonen, L., Uri, V., 2017. Digital photography for tracking the
338 phenology of an evergreen conifer stand. *Agricultural and Forest Meteorology* 246, 15-21.

339 Law, B.E., Van Tuyl, S., Cescatti, A., Baldocchi, D.D., 2001. Estimation of leaf area index in open-canopy
340 ponderosa pine forests at different successional stages and management regimes in Oregon.
341 *Agricultural and Forest Meteorology* 108, 1–14.

342 Leblanc, S.G., Chen, J.M., 2001. A practical scheme for correcting multiple scattering effects on optical LAI
343 measurements. *Agric. For. Meteorol.* 110, 125–139.

344 Liu, Z., Jin, G., Zhou, M., 2016. Evaluation and correction of optically derived leaf area index in different
345 temperate forests. *iForest-Biogeosciences and Forestry* 9, 55-62.

346 Macfarlane, C., Hoffman, M., Eamus, D., Kerp, N., Higginson, S., McMurtrie, R., Adams, M., 2007.
347 Estimation of leaf area index in eucalypt forest using digital photography. *Agricultural and Forest*
348 *Meteorology* 143 (3–4), 176–188.

349 Möttus, M., Stenberg, P., & Rautiainen, M. (2007). Photon recollision probability in heterogeneous forest
350 canopies: Compatibility with a hybrid GO model. *Journal of Geophysical Research — Atmospheres*,
351 112, D103104. <http://dx.doi.org/10.1029/2006JD007445>.

352 Myneni, R.B., Knyazikhin, Y., Privette, J.L., Glassy, J., Tian, Y., Wang, Y., et al., 2002. Global products of
353 vegetation leaf area and fraction absorbed PAR from year one of MODIS data. *Remote Sensing of*
354 *Environment* 83, 214–231.

355 Nasahara, K.N., Muraoka, H., Nagai, S., Mikami, H., 2008. Vertical integration of leaf area index in a
356 Japanese deciduous broad-leaved forest. *Agricultural and Forest Meteorology* 148 (6–7), 1136–1146.

357 Nilson, T., 1971. A theoretical analysis of the frequency of gaps in plant stands. *Agricultural Meteorology*
358 8, 25–38.

359 Noormets, A., Gavazzi, M.J., McNulty, S.G., Domec, J.-C., Sun, G., King, J.S., Chen, J., 2010. Response of
360 carbon fluxes to drought in a coastal plain loblolly pine forest. *Global Change Biology* 16, 272–287.

361 Norman, J.M., 1982, Simulation of microclimates, in *Biometeorology in Integrated Pest Management*,
362 edited by J.L. Hatfield and I.J. Thomason, pp. 65–99, Academic, San Diego, Calif.

363 Piayda, A., Dubbert, M., Werner, C., Vaz Correia, A., Pereira, J.S., Cuntz, M., 2015. Influence of woody
364 tissue and leaf clumping on vertically resolved leaf area index and angular gap probability estimates.
365 *For. Ecol. Manage.* 340, 103–113.

366 Pisek, J., Chen, J. M., Lacaze, R., Sonnentag, O., Alikas, K., 2010. Expanding global mapping of the foliage
367 clumping index with multi-angular POLDER three measurements: Evaluation and topographic
368 compensation. *ISPRS Journal of Photogrammetry and Remote Sensing* 65, 341–346.

369 Pisek, J., Ryu, Y., Sprintsin, M., He, L., Oliphant, A.J., Korhonen, L., Kuusk, J., Kuusk, A., Bergstrom, R.,
370 Verrelst, J., 2013a. Retrieving vegetation clumping index from Multiangle Imaging SpectroRadiometer
371 (MISR) data at 275m resolution. *Remote Sens. Environ.* 138, 126–133.

372 Pisek, J., Sonnentag, O., Richardson, A., & Möttus, M., 2013b. Is the spherical leaf inclination angle
373 distribution a valid assumption for temperate and boreal broadleaf tree species. *Agricultural and*
374 *Forest Meteorology* 169, 186–194.

375 Pisek, J., Govind, A., Arndt, S.K., Hocking, D., Wardlaw, T.J., Fang, H., Matteucci, G., Longdoz, B., 2015.
376 Intercomparison of clumping index estimates from POLDER, MODIS, and MISR satellite data over
377 reference sites. *ISPRS J. Photogramm. Remote Sens.* 101, 47–56.

378 Pueschel, P., Buddenbaum, H., Hill, J., 2012. An efficient approach to standardizing the processing of
379 hemispherical images for the estimation of forest structural attributes. *Agric. For. Meteorol.* 160, 1–
380 13.

381 Qu, Y., Meng, J., Wan, H., Li, Y., 2016. Preliminary study on integrated wireless smart terminals for leaf
382 area index measurement. *Computers and Electronics in Agriculture* 129, 56–65.

383 Raabe, K., Pisek, J., Sonnentag, O., Annuk, K., 2015. Variations of leaf inclination angle distribution with
384 height over the growing season and light exposure for eight broadleaf tree species. *Agric. For.*
385 *Meteorol.* 214-215, 2–11.

386 Rambal, S., Ourcival, J.M., Joffre, R., Mouillot, F., Nouvellon, Y., Reichstein, M., Rocheteau, A., 2003.
387 Drought controls over conductance and assimilation of a Mediterranean evergreen ecosystem:
388 scaling from leaf to canopy. *Global Change Biology* 9, 1813–1824.

389 Rautiainen, M., Möttöus, M., Stenberg, P., 2009. On the relationship of canopy LAI and photon recollision
390 probability in boreal forests. *Remote Sensing of Environment* 113, 458–461.

391 Ross, J., 1981. *The Radiation Regime and Architecture of Plant Stands*. Junk Publishers,
392 The Hague, 391 pp.

393 Ryu, Y., Nilson, T., Kobayashi, H., Sonnentag, O., Law, B.E., Baldocchi, D.D., 2010. On the correct
394 estimation of effective leaf area index: Does it reveal information on clumping effects? *Agricultural*
395 *and Forest Meteorology* 150, 463–472.

396 Ryu, Y., Baldocchi, D.D., Kobayashi, H., Ingen, C., Li, J., Black, T.A., Beringer, J., Gorsel, E., Knohl, A., Law,
397 B.E., 2011. Integration of MODIS land and atmosphere products with a coupled- process model to
398 estimate gross primary productivity and evapotranspiration from 1 km to global scales. *Global*
399 *Biogeochemical Cycles* 25, GB40117.

400 Serbin, S. P., Gower, S. T., & Ahl, D. E., 2009. Canopy dynamics and phenology of a boreal black spruce
401 wildfire chronosequence. *Agricultural and Forest Meteorology* 149, 187–204.

402 Shabanov, et al., 2003. Effect of foliage spatial heterogeneity in the MODIS LAI and FPAR algorithm over
403 broadleaf forests. *Remote Sensing of Environment* 85, 410–423.

404 Sinclair, T.R., Murphy, C.E., Knoerr, K.R., 1976. Development and evaluation of simplified models for
405 simulating canopy photosynthesis and transpiration. *Journal of applied Ecology* 13, 813-829.

406 Smolander, S., Stenberg, P., 2005. Simple parameterizations of the radiation budget of uniform
407 broadleaved and coniferous canopies. *Remote Sensing of Environment* 94, 355–363.

408

409 Solberg, S., Brunner, A., Hanssen, K.H., Lange, H., Næsset, E., Rautiainen, M., Stenberg, P., 2009. Mapping
410 LAI in a Norway spruce forest using airborne laser scanning. *Remote Sens. Environ.* 113, 2317–2327.

411 Sonnentag, O., van der Kamp, G., Barr, A.G. and Chen, J.M., 2010. On the relationship between water
412 table depth and water vapor and carbon dioxide fluxes in a minerotrophic fen. *Global Change Biology*
413 16, 1762-1776.

414 Sprintsin, M., Cohen, S., Maseyk, K., Rotenberg, E., Grunzweig, J., Karnieli, A., et al., 2011. Long term and
415 seasonal courses of leaf area index in a semi-arid forest plantation. *Agricultural and Forest*
416 *Meteorology* 151, 565–574.

417 Stenberg, P., 2007. Simple analytical formula for calculating average photon recollision probability in
418 vegetation canopies. *Remote Sensing of Environment* 109, 221–224.

419 Stenberg, P., Kangas, T., Smolander, H., Linder, S., 1999. Shoot structure, canopy openness, and light
420 interception in Norway spruce. *Plant, Cell and Environment* 22, 1133–1142.

421 Stenberg, P., Palmroth, S., Bond, B., Sprugel, D., Smolander, H., 2001. Shoot structure and photosynthetic
422 efficiency along the light gradient in a Scots pine canopy. *Tree Physiology* 21, 805–814.

423 Stenberg, P., Möttus, M., Rautiainen, M., 2016. Photon recollision probability in modelling the radiation
424 regime of canopies—a review. *Remote Sensing of Environment* 183, 98–108.

425 Taugourdeau, S., le Maire, G., Avelino, J., Jones, J.R., Ramirez, L.G., Jara Quesada, M., ...Roupsard, O.,
426 2014. Leaf area index as an indicator of ecosystem services and management practices: an application
427 for coffee agroforestry. *Agriculture, Ecosystems and Environment* 192, 19–37.

428 Talbot, J., Roulet, N.T., Sonnentag, O., Moore, T.R., 2014. Increases in aboveground biomass and leaf area
429 85 years after drainage in a bog, *Botany* 92, 713-721.

430 Tanaka, N., Kume, T., Yoshifuji, N., Tanaka, K., Takizawa, H., Shiraki, K., Tantasirin, C., Tangtham, N.,
431 Suzuki, M., 2008. A review of evapotranspiration estimates from tropical forests in Thailand and
432 adjacent regions. *Agricultural and Forest Meteorology* 148, 807–819.

433 Tedeschi, V., Rey, A., Manca, G., Valentini, R., Jarvis, P.G., Borghetti, M., 2006. Soil respiration in a
434 Mediterranean oak forest at different developmental stages after coppicing. *Global Change Biology*
435 12, 110–121.

436 Thimonier, A., Sedivy, I., & Schleppei, P., 2010. Estimating leaf area index in different types of mature forest
437 stands in Switzerland: A comparison of methods. *European Journal of Forest Research* 129,543–562.

438 Urbanski, S., Barford, C., Wofsy, S., Kucharik, C., Pyle, E., Budney, J., McKain, K., Fitzjarrald, D., Czikowsky,
439 M., Munger, J.W., 2007. Factors controlling CO₂ exchange on timescales from hourly to decadal at
440 Harvard Forest. *Journal of Geophysical Research-Biogeosciences* 112 (G02020),
441 doi:10.1029/2006JG000293.

442 Verger, A., Martínez, B., Coca, F. C. D., & García-Haro, F. J., 2009. Accuracy assessment of fraction of
443 vegetation cover and leaf area index estimates from pragmatic methods in a cropland area.
444 *International Journal of Remote Sensing*, 30, 2685–2704.

445 Vuolo, F., Neugebauer, N., Bolognesi, S.F., Atzberger, C., D'Urso, G., 2013. Estimation of leaf area index
446 using DEIMOS-1 data: application and transferability of a semi-empirical relationship between two
447 agricultural areas. *Remote Sensing* 5, 1274–1291.

448 Wei, S., Fang, H., 2016. Estimation of canopy clumping index from MISR and MODIS sensors using the
449 normalized difference hotspot and darkspot (NDHD) method: The influence of BRDF models and solar
450 zenith angle. *Remote Sensing of Environment* 187, 476-491.

451 Yan, K., Park, T., Yan, G., Chen, C., Yang, B., Liu, Z., Nemani, R., Knyazikhin, Y., Myneni, R., 2016a.
452 Evaluation of MODIS LAI/FPAR product collection 6. Part 1: consistency and Improvements. *Remote*
453 *Sensing* 8, 359.

- 454 Yan, K., Park, T., Yan, G., Liu, Z., Yang, B., Chen, C., Nemani, R., Knyazikhin, Y., Myneni, R., 2016b.
- 455 Evaluation of MODIS LAI/FPAR product collection 6. Part 2: validation and intercomparison. Remote
- 456 Sensing 8, 460.

Research highlights

- Synergy between a MODIS-based CI and a MODIS LAI product is examined
- Synergy assessed with spectral invariants theory, raw LAI-2000/2200 data
- It might be possible to obtain p -values for any location solely from EO data

1 Original research paper

2

3 **Data synergy between leaf area index and clumping index Earth Observation products**

4 **using photon collision probability theory**

5

6 Jan Pisek^{1*}, Henning Buddenbaum², Fernando Camacho³, Joachim Hill², Jennifer L.R.

7 Jensen⁴, Holger Lange⁵, Zhili Liu⁶, Arndt Piayda⁷, Yonghua Qu⁸, Olivier Roupsard⁹, Shawn

8 P. Serbin¹⁰, Svein Solberg⁵, Oliver Sonnentag¹¹, Anne Thimonier¹², Francesco Vuolo¹³

9 ¹Tartu Observatory, University of Tartu, 61602 Tõravere, Tartumaa, Estonia

10 ²Environmental Remote Sensing & Geoinformatics, Faculty of Environmental and
11 Regional Sciences, Trier University, D-54286 Trier, Germany

12 ³EOLAB, Parc Científic Universitat de València, c/ Catedràtic José Beltrán, 2. 46980
13 Paterna, Valencia, Spain

14 ⁴Department of Geography, Texas State University San Marcos, TX 7866, USA

15 ⁵Norwegian Institute of Bioeconomy Research, Ås, Akershus, Norway

16 ⁶Center for Ecological Research, Northeast Forestry University, Harbin 150040, China

17 ⁷Thünen Institute of Climate-Smart Agriculture, Bundesallee 65, 38116 Braunschweig,
18 Germany

19 ⁸State Key Laboratory of Remote Sensing Science, Beijing Key Laboratory for Remote
20 Sensing of Environment and Digital Cities, School of Geography, Beijing Normal
21 University, Beijing 100875, China

22 ⁹CIRAD-Persyst, UMR Ecologie Fonctionnelle and Biogéochimie des Sols et
23 Agroécosystèmes, SupAgro-CIRAD-INRA-IRD, Montpellier, France

24 ¹⁰Brookhaven National Laboratory, Environmental & Climate Sciences Department,
25 Upton, NY 11973-5000, USA

26 ¹¹Département de géographie and Centre d'études nordiques, Université de Montréal,
27 Montréal, QC H2V 2B8, Canada

28 ¹²WSL-Swiss Federal Institute for Forest, Snow and Landscape Research, Zürcherstrasse
29 111, 8903 Birmensdorf, Switzerland

30 ¹³Institute of Surveying, Remote Sensing and Land Information, Peter-Jordan-Straße 82
31 1190 Vienna, Austria

32 *Corresponding author. E-mail address: janpisek@gmail.com (J. Pisek)

33

34

35 **Abstract**

36 Clumping index (CI) is a measure of foliage aggregation relative to a random distribution
37 of leaves in space. The CI can help with estimating fractions of sunlit and shaded leaves
38 for a given leaf area index (LAI) value. Both the CI and LAI can be obtained from global
39 Earth Observation data from sensors such as the Moderate Resolution Imaging
40 Spectrometer (MODIS). Here, the synergy between a MODIS-based CI and a MODIS LAI
41 product is examined using the theory of spectral invariants, also referred to as photon
42 recollision probability (*p*-theory), along with raw LAI-2000/2200 Plant Canopy Analyzer
43 data from 75 sites distributed across a range of plant functional types. The *p*-theory
44 describes the probability (*p*-value) that a photon, having intercepted an element in the
45 canopy, will recollide with another canopy element rather than escape the canopy. We
46 show that empirically-based CI maps can be integrated with the MODIS LAI product. Our
47 results indicate that it is feasible to derive approximate *p*-values for any location solely
48 from Earth Observation data. This approximation is relevant for future applications of
49 the photon recollision probability concept for global and local monitoring of vegetation
50 using Earth Observation data.

51

52 **Keywords:** Photon recollision probability; Foliage clumping index; Leaf area index; Multi-
53 angle remote sensing

54

55

56 **1. Introduction**

57 Clumping index (CI) is a measure of foliage aggregation relative to a random
58 distribution of leaves in space (Nilson, 1971; Chen and Black, 1992). The CI is an
59 important factor for the correct quantification of true leaf area index (LAI). The CI is also
60 needed for estimating fractions of sunlit and shaded leaves in the canopy (Norman,
61 1982) - an effective way for upscaling from leaf to canopy for modeling vegetation
62 photosynthesis (Bonan et al., 2014; He et al., 2017; Jiang and Ryu, 2016). Global and
63 regional scale CI maps have been generated from various multi-angle sensors (e.g. He et
64 al., 2012; Pisek et al., 2010; 2013a; Wei and Fang, 2016) based on an empirical
65 relationship with the normalized difference between hotspot and darkspot (NDHD)
66 index (Chen et al., 2005). Ryu et al. (2011) suggested that the adequate representation
67 of canopy radiative transfer, important for the simulation of gross primary productivity
68 and evapotranspiration (Baldocchi and Harley, 1995), is possible by integrating CI with
69 incoming solar irradiance and LAI from Moderate Resolution Imaging Spectrometer
70 (MODIS) land and atmosphere products. It should be noted that the MODIS LAI/FPAR
71 product (MOD15A2H) uses internal a set of non-empirical, stochastic equations for the
72 parameterization of foliage clumping (Shabanov et al., 2003). Our objective is to find out
73 if the MODIS LAI product with its non-empirical, stochastic clumping parameterization
74 can be used together with empirically-based CI maps, e.g. for the calculation of
75 sunlit/shaded fractions of LAI.

76 Here, we assess the synergy between a MODIS-based CI (He et al., 2012) and a
77 MODIS LAI product (Yan et al., 2016a,b) using the theory of spectral invariants or 'p-
78 theory' (Knyazikhin et al., 1998) along with raw LAI-2000/2200 Plant Canopy Analyzer

79 (PCA; LI-COR Biosciences, Lincoln, NE, USA) data from 75 sites surveyed across a range
80 of plant functional types (PFTs). The p -theory predicts that the amount of radiation
81 scattered (reflected or transmitted) within a canopy depends only on the wavelength
82 and the spectrally invariant canopy structural parameter p . It can be interpreted as the
83 probability of a photon, having intercepted an element in the canopy, to recollide with
84 another canopy element rather than escape the canopy (Smolander and Stenberg,
85 2005). The parameter p is linked to the foliage clumping (Stenberg et al., 2016).
86 Simulation studies by Möttus et al. (2009) and Smolander and Stenberg (2005) showed
87 the recollision probability is closely related to LAI, with p -LAI relationships varying with
88 the degree of clumping in the spatial distribution of leaf (needle) area. At a fixed LAI, p -
89 value is larger the more aggregated the leaves in a canopy, or the smaller the canopy Cl.
90 The p -theory is intuitive and connected to the radiative transfer theory through the
91 eigenvalues of the radiative transfer equation (Knyazikhin et al., 1998). Stenberg et al.
92 (2016) provide an excellent review of the photon recollision probability concept in
93 modelling the radiation regime of canopies.

94

95 **2. Materials and methods**

96 2.1 Method

97 Stenberg (2007) proposed to approximate a photon recollision probability for a
98 canopy (p -value) from the Plant Canopy Analyzer (PCA) as:

$$99 \quad p = 1 - (i_0 / LAI_{true}) \quad (1)$$

100 where p is photon recollision probability, LAI_{true} is true leaf area index, and i_0 is canopy
 101 interception (the portion of the incoming radiation (photons) that is intercepted by the
 102 leaves), which can be expressed as:

$$103 \quad i_0 = 1 - t_0 \quad (2)$$

104 where i_0 and t_0 are canopy interception and transmittance under diffuse, isotropic
 105 illumination conditions with constant directional intensity (Stenberg, 2007). Both i_0 and
 106 t_0 describe first interactions (with the canopy or the ground) only, and do not include
 107 photons which escape or interact again after being scattered from a leaf or the ground
 108 (Stenberg, pers. comm). Stenberg (2007) and Smolander and Stenberg (2005) further
 109 assume the canopy to have spherical leaf/shoot orientation and to be bounded
 110 underneath by a non-reflecting surface. t_0 is obtained as:

$$111 \quad t_0 = 2 \int_0^{\frac{\pi}{2}} \overline{cgf}(\theta) \sin(\theta) \cos(\theta) d\theta \quad (3)$$

112 where \overline{cgf} is the canopy gap fraction at zenith angle θ (averaged over azimuth angle
 113 and horizontal area). Eqs. (1,2) can be combined to give:

$$114 \quad p = 1 - \frac{1 - 2 \int_0^{\frac{\pi}{2}} \overline{cgf}(\theta) \sin(\theta) \cos(\theta) d\theta}{LAI_{true}} \quad (4)$$

115 It should be noted that p as defined by Stenberg (2007) is a canopy structural
 116 characteristic which is independent of the above canopy radiation conditions. The PCA-
 117 based LAI estimate (LAI_{PCA}) is calculated here as the mean of the logarithms of the gap
 118 fraction values with clumping effects partially considered (Ryu et al., 2010):

$$119 \quad LAI_{PCA} = -2 \int_0^{\frac{\pi}{2}} \overline{\ln(cgf(\theta))} \sin(\theta) \cos(\theta) d\theta \quad (5)$$

120 For the coniferous sites, the PCA estimate (LAI_{PCA}) is further converted to true LAI using
121 a shoot-scale grouping correction factor γ_E ($LAI_{true}=LAI_{PCA}*\gamma_E$) before calculating p
122 (Rautiainen et al., 2009).

123 Alternatively, t_0 can be also estimated for an effective zenith angle θ as a
124 function of LAI, mean projection of unit foliage area (G) (Ross, 1981), and clumping
125 index (CI) (Chen et al., 2005):

$$126 \quad t_0(\theta)=\exp[-G(\theta)CI LAI_{true}/\cos\theta] \quad (6)$$

127 Combining Eqs. (1) and (2) with (6), photon recollision probability p can then be
128 calculated with CI and LAI estimated from Earth Observation data as:

$$129 \quad p=1-(1-\exp[-G(\theta)CI LAI_{true}/\cos\theta])/LAI_{true} \quad (7)$$

130 with $G(\theta)=0.5$ and θ set as 57.3° to minimize the uncertainty about leaf angle
131 orientation information (Pisek et al., 2013b) and assuming that t_0 in Eq. (2) for the upper
132 hemisphere can be approximated by $t_0(57.3^\circ)$. Eqs. (4) and (7) provide a simple way to
133 evaluate the synergy of MODIS LAI (Yan et al., 2016a) and CI (He et al., 2012) products
134 with independent PCA estimates. In case of needleleaf forests, Eq. (7) needs to be
135 further modified when used in combination with the MODIS LAI product (LAI_{MODIS}):

$$136 \quad p=1-(1-\exp[-G(\theta) CI \gamma_E LAI_{MODIS}/\cos\theta])/(LAI_{MODIS} \gamma_E) \quad (8)$$

137 as vegetation clumping is not accounted for at the shoot scale in the original MODIS LAI
138 product (Yan et al., 2016b).

139

140 2.2 MODIS LAI data

141 The current version of the MODIS LAI/FPAR product (MOD15A2H) is Collection 6
142 (C6) (Yan et al., 2016a). The main algorithm is based on look-up tables (LUTs) simulated
143 from a three-dimensional radiative transfer (3D RT) model (Knyazikhin et al., 1999;
144 Myneni et al., 2002). The algorithm finds the best LAI and FPAR estimates with biome-
145 specific LUTs using daily land surface Bi-directional Reflectance Factors (BRFs) along with
146 their uncertainties. A back-up empirical method utilizes relationships between the
147 Normalized Difference Vegetation Index and LAI/FPAR to produce lower quality LAI
148 estimates. The LAI value corresponding to the maximum FPAR is selected over the
149 compositing period of four or eight days. Vegetation clumping in the 3D RT is accounted
150 for at plant and canopy scales.

151 The most important improvement in MOD15A2H C6 compared to previous
152 versions is the increase from 1 km to 500 m spatial resolution. In addition, a new version
153 of MODIS surface reflectances (MOD09GA C6) is used to replace the previous 1 km
154 intermediate dataset (MODAGAGG). In C6 the 1 km static land cover input is replaced
155 with new multi-year MODIS land cover product (MCD12Q1) at 500 m resolution.

156 Only MODIS LAI retrievals produced with the main RT algorithm closest to the
157 date of PCA measurements (see Section 2.4) were used in this study.

158

159 2.3 MODIS CI data

160 He et al. (2012) derived a global CI map at 500 m spatial resolution using the red
161 band (620-670 nm) from the MODIS BRDF Model Parameters product (MCD43A1;
162 Schaaf et al., 2002). Since MODIS does not observe near the hotspot and the angular

163 kernels used to construct the MODIS BRDF product do not include the complete hotspot
164 physics and consistently underestimate the hotspot, He et al. (2012) developed an
165 approach to correct the MODIS hotspot magnitude with synchronous co-registered
166 POLDER-3 data. After the MODIS hotspot correction, CI is derived using two coefficients
167 calculated from the second-order polynomial fit of the tabulated relationship between
168 CI and NDHD by Chen et al. (2005). He et al. (2012) assigned a single annual CI value, the
169 median from its noisy seasonal trajectory, to each pixel in the final map. This global CI
170 map is provided using the same pixel grid and projection as the MODIS LAI product
171 (Section 2.2).

172

173 2.4 Plant Canopy Analyzer data

174 Ryu et al. (2010) compiled raw PCA instrument data from 41 sites distributed
175 across six plant functional types ranging from boreal to tropical ecoclimatic zones. PCA
176 data from 34 sites from their synthesis data set were retained after assessing their
177 suitability for our study (e.g. representativeness of the area at the scale of
178 corresponding overlapping 500 m MODIS pixel footprint verified with Google Earth
179 Engine (Gorelick et al., 2017); temporal overlap with MODIS LAI product) (Table 1). In
180 addition to the retained sites from Ryu et al. (2010), PCA measurements from 41
181 additional sites were included in this study. The available raw PCA data were used to
182 approximate p -value at each site using Eq. (4). The corresponding γ_E values for given
183 coniferous species were obtained from literature and are provided in Table 1.

184 Table 1. Characteristics and results for 75 sites with raw PCA measurements. PFT is plant
185 functional type. Lat is latitude (in degrees). Lon is longitude (in degrees). PCA is Plant

186
187

Canopy Analyzer. LAI_{PCA} is LAI estimate from PCA data. p is the photon recollision probability. γ_E is the needle-to-shoot area ratio.

PFT	Country	Site name	Lat	Lon	Species	raw PCA data source	LAI_{PCA}	t_0	p	γ_E
CRO	Austria	Marchfeld_B	48.16N	16.7E	Beet	Vuolo et al. (2016)	2.87	0.095	0.72	
CRO	Austria	Marchfeld_M	48.18N	16.92E	Maize	Vuolo et al. (2016)	3.10	0.089	0.72	
CRO	Austria	Marchfeld_W	48.18N	16.91E	Wheat	Vuolo et al. (2016)	0.55	0.683	0.48	
CRO	China	Heilongjiang	48.13N	126.96E	Corn	Qu et al. (2016)	0.72	0.548	0.42	
CRO	Costa Rica	Aquiaries	9.93N	83.71W	Coffee	Taugordeau et al. (2014)	2.66	0.107	0.70	
CRO	Japan	Nagaoka	37.48N	138.78E	Rice – early planted	Kobayashi (unpublished)	2.72	0.124	0.70	
CRO	Japan	Nagaoka	37.48N	138.78E	Rice – later planted	Kobayashi (unpublished)	2.84	0.111	0.71	
CRO	Spain	Barrax C-3	39.06N	2.09W	Corn	Verger et al. (2009)	0.36	0.746	0.35	
CRO	Spain	Barrax C-2	39.05N	2.09W	Corn	Verger et al. (2009)	0.42	0.715	0.37	
DBF	Estonia	Järvelja	58.29N	27.26E	Silver birch	Kodar et al. (2008)	3.78	0.081	0.76	
DBF	Germany	Hohes Holz	52.08N	11.22E	Beech	Piayda (unpublished)	4.44	0.025	0.79	
DBF	Germany	Merzalben	49.26N	7.8E	Beech, oak	Pueschel et al. (2012)	4.24	0.029	0.77	
DBF	Italy	Ro1	42.41N	11.93E	Oak	Tedeschi et al. (2006)	3.70	0.052	0.75	
DBF	Italy	Ro2	42.39N	11.92E	Oak	Tedeschi et al. (2006)	4.57	0.028	0.79	
DBF	Japan	Takayama	36.14N	137.42E	Mongolian oak	Nasahara et al. (2008)	3.66	0.045	0.74	
DBF	Korea	Gwangneung	37.76N	127.15E	Oak	Kwon (unpublished)	4.57	0.018	0.79	
DBF	Switzerland	Bettlachstock	47.23N	7.41E	Beech	Thimonier et al. (2010)	4.53	0.02	0.79	
DBF	Switzerland	Isonne	46.13N	9.01E	Beech	Thimonier et al. (2010)	3.81	0.035	0.76	
DBF	Switzerland	Lausanne	46.58N	6.66E	Beech	Thimonier et al. (2010)	5.45	0.012	0.82	
DBF	Switzerland	Neunkirch	47.68N	8.53E	Beech	Thimonier et al. (2010)	3.76	0.04	0.75	
DBF	Switzerland	Schänis	47.16N	9.06E	Beech	Thimonier et al. (2010)	4.07	0.03	0.76	
DBF	Switzerland	Novaggio	46.01N	8.83E	Oak	Thimonier et al. (2010)	3.21	0.059	0.72	
DBF	Switzerland	Jussy	46.23N	6.28E	Oak, hornbeam	Thimonier et al. (2010)	4.12	0.031	0.78	
DBF	USA	Chestnut	35.93N	84.45W	Chestnut	Heuer (unpublished)	3.53	0.052	0.73	
DBF	USA	Harvard	42.53N	72.17W	Oak	Urbanski et al. (2007)	4.69	0.022	0.79	
DBF	USA	Coweeta	35.05N	83.45W	Oak-hickory	Hwang et al. (2009)	5.51	0.03	0.83	
EBF	France	Puechabon	43.74N	3.6E	Oak	Rambal et al. (2003)	3.06	0.081	0.70	
EBF	Portugal	Coruche	39.13N	8.33W	Oak	Piayda et al. (2015)	0.73	0.559	0.49	
EBF	Thailand	Kog-Ma	18.8N	98.9E	Lithocarpus	Tanaka et al. (2008)	3.65	0.048	0.74	
ENF	Canada	Scotty Creek	61.31N	121.3W	Black spruce	Sonnentag (unpublished)	0.83	0.514	0.75	1.36
ENF	Canada	Thompson_1850	55.87N	98.47W	Black spruce	Serbin et al. (2009)	2.28	0.206	0.73	1.36
ENF	Canada	Thompson_1930	55.89N	98.51W	Black spruce	Serbin et al. (2009)	2.07	0.214	0.63	1.36
ENF	Canada	Campbell river	49.51N	124.9W	Douglas fir - young	Chen et al. (2006)	2.75	0.108	0.82	1.66
ENF	Estonia	Järvelja	58.3N	27.24E	Norway spruce	Kodar et al. (2008)	3.12	0.095	0.82	1.42
ENF	Estonia	Järvelja	58.3N	27.26E	Scots pine	Kodar et al. (2008)	2.51	0.156	0.80	1.7
ENF	Korea	Gwangneung	37.76N	127.16E	Korean pine	Kwon (unpublished)	4.44	0.021	0.76	1.21
ENF	Norway	Østmarka_1	59.81N	11.0E	Norway spruce	Solberg et al. (2009)	2.17	0.216	0.70	1.42
ENF	Norway	Østmarka_2	59.81N	10.99E	Norway spruce	Solberg et al. (2009)	1.17	0.488	0.87	1.42
ENF	Norway	Østmarka_3	59.82N	11.0E	Norway spruce	Solberg et al. (2009)	5.17	0.021	0.81	1.42
ENF	Norway	Østmarka_5	59.82N	11.02E	Norway spruce	Solberg et al. (2009)	3.26	0.09	0.81	1.42
ENF	Norway	Østmarka_6	59.82N	11.02E	Norway spruce	Solberg et al. (2009)	3.28	0.085	0.84	1.42
ENF	Norway	Østmarka_7	59.81N	11.02E	Norway spruce	Solberg et al. (2009)	4.07	0.05	0.80	1.42
ENF	Norway	Østmarka_8	59.83N	11.03E	Norway spruce	Solberg et al. (2009)	3.11	0.096	0.79	1.42
ENF	Norway	Østmarka_9	59.83N	11.01E	Norway spruce	Solberg et al. (2009)	2.88	0.117	0.80	1.42
ENF	Norway	Østmarka_6_2003	59.82N	11.02E	Norway spruce	Solberg et al. (2009)	3.15	0.104	0.87	1.42
ENF	Norway	Østmarka_3_2003	59.82N	11.0E	Norway spruce	Solberg et al. (2009)	5.27	0.019	0.68	1.42
ENF	Norway	Østmarka_2_2003	59.81N	10.99E	Norway spruce	Solberg et al. (2009)	0.95	0.561	0.78	1.42
ENF	Norway	Østmarka_1_2003	59.81N	11.0E	Norway spruce	Solberg et al. (2009)	2.13	0.219	0.75	1.42
ENF	Switzerland	Alptal	47.05N	8.71E	Norway spruce	Thimonier et al. (2010)	2.73	0.1	0.77	1.42
ENF	Switzerland	Chironico	46.45N	8.81E	Norway spruce	Thimonier et al. (2010)	2.60	0.109	0.72	1.42
ENF	Switzerland	Lens	46.26N	7.43E	Scots pine	Thimonier et al. (2010)	2.09	0.164	0.67	1.7
ENF	Switzerland	Visp	46.3N	7.86E	Scots pine	Thimonier et al. (2010)	1.58	0.248	0.78	1.7
ENF	Switzerland	Vordemwald	47.28N	7.88E	Silver fir	Thimonier et al. (2010)	3.64	0.05	0.79	1.91
ENF	USA	US-NC2	35.48N	76.4W	Loblolly pine	Noormets et al. (2009)	4.23	0.034	0.87	1.21
ENF	USA	Howland	45.21N	68.74W	Red spruce	Richardson (unpublished)	1.94	0.2	0.81	1.6
ENF	USA	SJ57	47.13N	116.18W	Cedar, spruce, larch, pine	Jensen et al. (2011)	2.18	0.175	0.65	1.01
ENF	USA	527	46.22N	116.79W	Fir, pine, spruce, larch	Jensen et al. (2011)	1.94	0.189	0.59	1.01

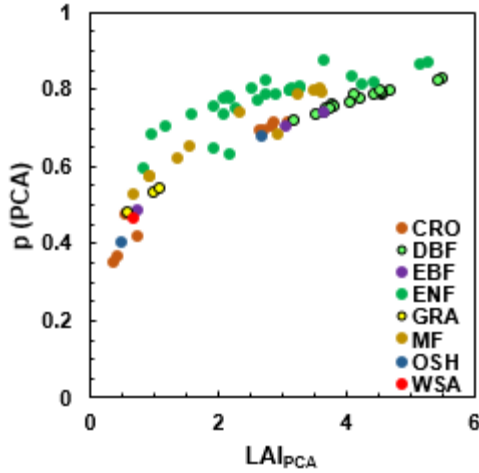
GRA	Canada	Sandhill	53.79N	104.62W	Sedges	Sonnentag et al. (2010)	1.10	0.459	0.54
GRA	USA	Vaira	38.41N	120.95W	Annual grass	Ryu et al. (2010)	0.99	0.416	0.53
GRA	USA	Sherman	38.04N	121.75W	Invasive weed	Sonnentag (unpublished)	0.61	0.641	0.48
MF	Canada	Timins	48.21N	82.15W	Aspen, spruce, birch, fir	Chen et al. (2006)	3.50	0.068	0.80 1.36
MF	Canada	Thompson_1964	55.91N	98.38W	Spruce, pine, aspen, willow	Serbin et al. (2009)	1.55	0.305	0.65 1.36
MF	Canada	Thompson_1981	55.85N	98.85W	Willow, jack pine, aspen	Serbin et al. (2009)	1.35	0.352	0.62 1.36
MF	Canada	Thompson_1989_1	55.90N	98.95W	Willow, jack pine, aspen	Serbin et al. (2009)	0.91	0.489	0.58 1.36
MF	Canada	Thompson_1989_2	55.91N	98.97W	Willow, jack pine, aspen	Serbin et al. (2009)	0.91	0.489	0.58 1.36
MF	Canada	Thompson_1994	56.16N	96.71W	Willow, jack pine, aspen	Serbin et al. (2009)	0.68	0.578	0.53 1.36
MF	China	SB	47.19N	128.87E	Birch, larch, pine	Liu et al. (2016)	2.32	0.179	0.74 1.08
MF	China	SC	47.19N	128.89E	Pine, birch, beech, elm	Liu et al. (2016)	3.60	0.053	0.80 1.28
MF	China	KP	47.18N	128.88E	Pine, birch, larch	Liu et al. (2016)	3.23	0.086	0.79 1.46
MF	China	BK	47.18N	128.9E	Pine, birch, maple, tilia	Liu et al. (2016)	3.62	0.054	0.80 1.41
MF	Estonia	Järvselja	58.29N	27.25E	Birch, spruce	Kodar et al. (2008)	3.59	0.06	0.81 1.42
MF	USA	WPA	47.63N	122.29W	Fir, maple, cedar, hemlock	Richardson et al. (2009)	2.91	0.082	0.68 1.36
OSH	Canada	Mer Bleue	45.4N	75.5W	Shrub (peatland)	Talbot et al. (2014)	2.69	0.104	0.68
OSH	Canada	Thompson_2003	55.9N	98.18W	Wild rose, fireweed	Serbin et al. (2009)	0.48	0.671	0.41
WSA	USA	Tonzi	38.43N	120.97W	Blue oak	Ryu et al. (2010)	0.68	0.583	0.47

CRO: crop, DBF: deciduous broadleaf forest, EBF: evergreen broadleaf forest, ENF: evergreen needleleaf forest, GRA: grass, MF: mixed forest, OSH: open shrubland, WSA: woody savanna.

188
189
190
191

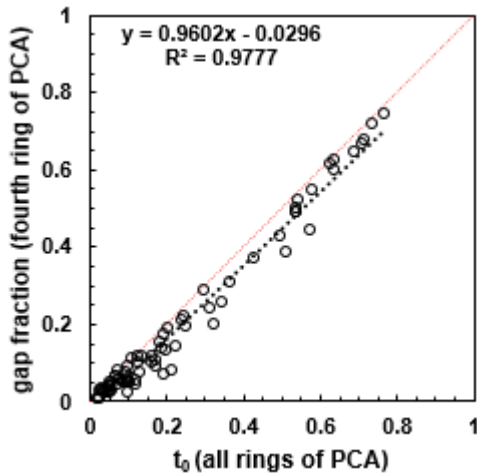
3. Results and Discussion

192 The relationship between LAI and photon recollision probability p approximated
193 with PCA data using Eq. (4) is shown in Fig. 1. The nature of the p -LAI_{PCA} relationship is
194 different between evergreen needleleaf (ENF) and other PFTs due to the inclusion of the
195 shoot-scale correction factor (Chen, 1996). Compared to Rautiainen et al. (2009), the p -
196 values representing needleleaf stands with greater variety of tree species were more
197 dispersed. Our results support the notion by Rautiainen et al. (2009) that establishing
198 species-specific p -LAI_{PCA} functions would require further research on the role of shoot-
199 scale (shoot level) clumping and its documented variability between species (e.g. Chen
200 et al., 2006; Stenberg et al., 1999; 2001) on photon recollision probability.



201

202 **Fig. 1.** Relationship between Plant Canopy Analyzer (PCA)-derived leaf area index
 203 (LAI_{PCA}) and approximated photon recollision probability p . The abbreviations used in
 204 the figure legend are explained in the caption of Table 1.
 205



206

207 **Fig. 2.** Comparison between the transmittance (t_0 ; Eq. (3)) and gap fraction from the
 208 fourth ring of Plant Canopy Analyzer (PCA) data.

209

210 Eq. (7) assumes that t_0 in Eq. (3) for the upper hemisphere can be approximated

211 by $t_0(57.3^\circ)$. A regression between the gap fraction from the fourth ring (47–58° from

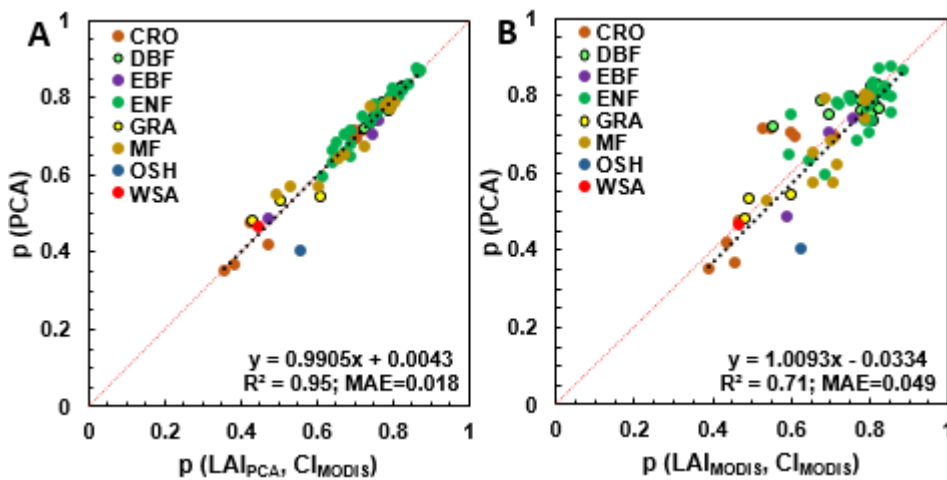
212 zenith) and t_0 obtained from all five rings (Eq. (3)) for all sites is shown in Fig. 2. The tight

213 linear relationship close to the 1:1 line indicates that this ring alone (or 57.3° as its

214 representative) is indeed a reasonable approximation for t_0 of the upper hemisphere,

215 while simultaneously reducing the uncertainty introduced through an assumed leaf
 216 inclination angle distribution. It should be noted that previous research by Leblanc and
 217 Chen (2001) also found that the fourth ring itself provides a good approximation of
 218 LAI_{PCA} under both direct and diffuse light conditions.

219 Fig. 3A shows a strong linear relationship ($R^2=0.95$; Mean Absolute Error (MAE)=
 220 0.018; intercept 0.0043) between the p -values derived from Eqs. (4) and (7)



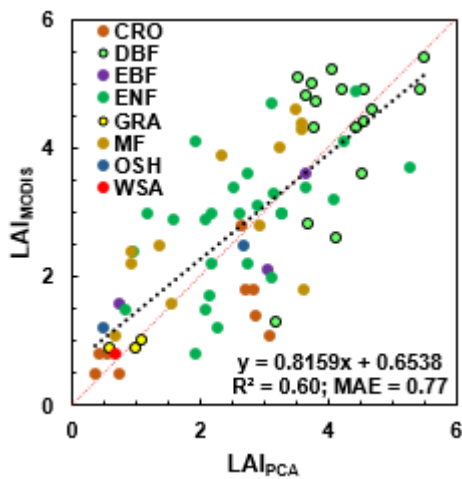
221

222 **Fig. 3.** Relationships between photon recollision probabilities p derived with Eqs. (4) and
 223 (7) using Plant Canopy Analyzer (PCA) data (A) and MODIS LAI C6 product (B) as LAI
 224 input into Eq. (7).

225

226 using the PCA and γ_E data from Table 1 as the source of information about LAI, and CI
 227 values retrieved from He et al. (2012). Fig. 3A confirms the agreement between the two
 228 approaches (Eqs. (4) and (7)) to obtain p -value. The observed variation stems mainly
 229 from the uncertainty in G-function, CI values and approximation of $t_0(57.3^\circ)$ to t_0 of the
 230 upper hemisphere (Fig. 2). The clumping may change with season (Sprintsin et al., 2011;
 231 Pisek et al., 2015; Lang et al., 2017), while He et al. (2012) provide only the seasonal
 232 trajectory median value.

233 The linear relationship close to the 1:1 line (slope 1.0093; intercept -0.034)
 234 between the p -values derived from PCA and MODIS-only data (Fig. 3B) suggests a
 235 general compatibility of MODIS LAI and CI maps by He et al. (2012). Our results supports
 236 that a) the MODIS algorithm indeed uses the recollision probability to account for
 237 clumping, and b) the approach integrating the empirically based CI information with
 238 MODIS LAI suggested by Ryu et al. (2011) appears to be feasible. The difference
 239 between Figs. 3A and 3B is the inclusion of the MODIS LAI product in the latter one.
 240 Since the clumping in MODIS LAI is accounted for at the plant and canopy scales only,
 241 knowledge about the shoot-scale grouping correction factor γ_E is needed to retrieve the
 242 non-underestimated p -values in case of needleleaf forests.
 243



244
 245 **Fig. 4.** Relationship between Plant Canopy Analyzer (PCA)-derived leaf area index
 246 (LAI_{PCA}) and MODIS LAI C6 product (LAI_{MODIS}). Both PCA and MODIS LAI data are not
 247 corrected for the shoot-scale grouping correction factor γ_E .

248
 249 Fig. 4 shows the scatterplot between LAI estimates from PCA and MODIS LAI C6
 250 product. The increase in mean absolute error in Fig. 3B (MAE=0.049) compared to Fig.
 251 3A (MAE=0.018) is linked to the different estimates and sources of LAI information for

252 Eq. (4) (PCA) and Eqs. (7) and (8) (MODIS LAI) as illustrated in Fig. 4. Furthermore, Fig. 1
253 shows that accurate LAI information for photon recollision probability estimation is
254 particularly critical at lower LAI values. Since reflectance values are not saturated within
255 LAI range of 0-2, LAI algorithms perform well within this domain (Yan et al., 2016b) and
256 should be able to provide high quality input data. Importantly, it should be verified if the
257 LAI input indeed corresponds to true LAI.

258 Our findings illustrate that it might be possible to obtain approximate p -values
259 for any location solely from Earth Observation data, given availability of high quality LAI
260 retrievals. In the future, the relationship could be possibly strengthened by further
261 improved CI retrieval algorithms from Earth Observation data (e.g. Wei and Fang, 2016),
262 by accounting for seasonal variation of clumping (He et al., 2016) and by knowing site
263 specific G-function values (Raabe et al., 2015). It is envisioned that our findings provide a
264 stimulus for future applications of the photon recollision probability concept for global
265 and local monitoring of vegetation using Earth Observation data (Stenberg et al., 2016).

266

267 **4. Conclusion**

268 Our results indicate that the integration of a MODIS LAI product with empirically-
269 based CI maps is feasible. Their synergy was assessed using the p -theory along with raw
270 LAI-2000/2200 Plant Canopy Analyzer data gathered across a wide range of plant
271 functional types. Importantly, for the first time it is shown that it might be possible to
272 obtain approximate p -values for any location solely from Earth Observation data. This
273 approximation is relevant for future applications of photon recollision probability

274 concept for global and local monitoring of vegetation using Earth Observation data
275 (Stenberg et al., 2016).

276

277 **Acknowledgements**

278 JP was supported by Estonian Research Council Grant PUT1355 and Mobilitas Pluss
279 MOBERC11. The global clumping index map by He et al. (2012) is available for download
280 through the following link:

281 [https://www.researchgate.net/publication/314151326 Global Clumping Index Map.](https://www.researchgate.net/publication/314151326_Global_Clumping_Index_Map)

282 The MODIS LAI C6 data have been accessed through Google Earth Engine. Dr. Youngryel
283 Ryu kindly shared his compilation of raw PCA data. Original providers of the raw PCA
284 data to Dr. Ryu are appreciated: Drs. Jing Ming Chen, Michael Gavazzi, Mark Heuer,
285 Taehee Hwang, Joon Kim, Soo-Hyung Kim, Hideki Kobayashi, John Kochendorfer,
286 Hyojung Kwon, Beverly Law, Craig Macfarlane, Francesco Mazzenga, Mark Mesarch,
287 William Munger, Kenlo Nishida Nasahara, Asko Noormets, Jean-Marc Ourcival, Dario
288 Papale, Serge Rambal, Andrew Richardson, Julie Talbot, Shashi Verma, and Leland
289 Werden. Drs. Martin Béland, Yuri Knyazikhin, Philip Lewis and Pauline Stenberg provided
290 valuable input and comments on the concept provided in this study. Authors wish to
291 thank three anonymous reviewers for constructive comments on the manuscript.

292

293 **References**

294 Baldocchi, D.D., Harley, P.C., 1995. Scaling carbon dioxide and water vapour exchange from leaf to canopy
295 in a deciduous forest. II. Model testing and application. *Plant, Cell & Environment* 18, 1157–1173.

296 Bonan, G. B., Williams, M., Fisher, R. A., & Oleson, K. W. (2014). Modeling stomatal conductance in the
297 earth system: linking leaf water-use efficiency and water transport along the soil-plant-atmosphere
298 continuum. *Geoscientific Model Development*, 7, 2193-2222. doi:10.5194/gmd-7-2193-2014.

299 Burba, G.G., Verma, S.B., 2005. Seasonal and interannual variability in evapotranspiration of native
300 tallgrass prairie and cultivated wheat ecosystems. *Agricultural and Forest Meteorology* 135 (1–4),
301 190–201.

302 Chen, J.M., 1996. Optically-based methods for measuring seasonal variation of leaf area index in boreal
303 conifer stands. *Agricultural and Forest Meteorology* 80, 135–163.

304 Chen, J.M., Black, T.A., 1992. Foliage area and architecture of plant canopies from sunfleck size
305 distributions. *Agricultural and Forest Meteorology* 60, 249–266.

306 Chen, J.M., Menges, C.H., Leblanc, S.G., 2005. Global mapping of foliage clumping index using multi-
307 angular satellite data. *Remote Sensing of Environment* 97, 447–457.

308 Chen, J.M., Govind, A., Sonnentag, O., Zhang, Y.Q., Barr, A., Amiro, B., 2006. Leaf area index
309 measurements at Fluxnet-Canada forest sites. *Agricultural and Forest Meteorology* 140, 257–268.

310 Gorelick, N., Hancher, M., Dixon, M., Ilyushchenko, S., Thau, D., Moore, R., 2017. Google earth engine:
311 Planetary-scale geospatial analysis for everyone. *Remote Sensing of Environment* 202, 18-27.

312 He, L., Chen, J.M., Pisek, J., Schaaf, C.B., Strahler, A.H., 2012. Global clumping index map derived from the
313 MODIS BRDF product. *Remote Sensing of Environment* 119, 118–130.

314 He, L., Liu, J., Chen, J.M., Croft, H., Wang, R., Sprintsin, M., Zheng, T., Ryu, Y., Pisek, J., Gonsamo, A., Deng,
315 F., and Zhang, Y. (2016). Inter- and intra-annual variations of clumping index derived from the MODIS
316 BRDF product. *International Journal of Applied Earth Observation and Geoinformation*, 44, 53-60.

317 He, L., Chen, J. M., Croft, H., Gonsamo, A., Luo, X., Liu, J., . . . Liu, Y. (2017). Nitrogen Availability Dampens
318 the Positive Impacts of CO₂ Fertilization on Terrestrial Ecosystem Carbon and Water Cycles.
319 *Geophysical Research Letters*, n/a-n/a. doi:10.1002/2017GL075981.

320 Hwang, T., Band, L.E., Hales, T.C., 2009. Ecosystem processes at the watershed scale: extending optimality
321 theory from plot to catchment. *Water Resources Research* 45 (W11425),
322 doi:10.1029/2009WR007775.

323 Jensen, J. L. R., Humes, K. S., Vierling, L. A., & Hudak, A. T., 2008. Discrete return lidar-based prediction of
324 leaf area index in two conifer forests. *Remote Sensing of Environment* 112, 3947–3957.

325 Jiang, C., & Ryu, Y. (2016). Multi-scale evaluation of global gross primary productivity and
326 evapotranspiration products derived from Breathing Earth System Simulator (BESS). *Remote Sensing*
327 *of Environment*, 186, 528-547.

328 Knyazikhin, Y.; Glassy, J.; Privette, J.L.; Tian, Y.; Lotsch, A.; Zhang, Y.; Wang, Y.; Morisette, J.T.; Votava, P.;
329 Myneni, R.B., 1999. MODIS Leaf Area Index (LAI) and Fraction of Photosynthetically Active Radiation
330 Absorbed by Vegetation (FPAR) Product (MOD15) Algorithm Theoretical Basis Document; Theoretical
331 Basis Document; NASA Goddard Space Flight Center: Greenbelt, MD, USA, 1999; p. 20771.

332 Knyazikhin, Y., Martonchik, J., Myneni, R., Diner, D., Running, S., 1998. Synergistic algorithm for estimating
333 vegetation canopy leaf area index and fraction of absorbed photosynthetically active radiation from
334 MODIS and MISR data. *Journal of Geophysical Research* D103(32), 257–32 276.

335 Kodar, A., Kutsar, R., Lang, M., Lukk, T., Nilson, T., 2008. Leaf area indices of forest canopies from optical
336 measurements. *Baltic Forestry* 14 (2), 185–194.

337 Lang, M., Nilson, T., Kuusk, A., Pisek, J., Korhonen, L., Uri, V., 2017. Digital photography for tracking the
338 phenology of an evergreen conifer stand. *Agricultural and Forest Meteorology* 246, 15-21.

339 Law, B.E., Van Tuyl, S., Cescatti, A., Baldocchi, D.D., 2001. Estimation of leaf area index in open-canopy
340 ponderosa pine forests at different successional stages and management regimes in Oregon.
341 *Agricultural and Forest Meteorology* 108, 1–14.

342 Leblanc, S.G., Chen, J.M., 2001. A practical scheme for correcting multiple scattering effects on optical LAI
343 measurements. *Agric. For. Meteorol.* 110, 125–139.

344 Liu, Z., Jin, G., Zhou, M., 2016. Evaluation and correction of optically derived leaf area index in different
345 temperate forests. *iForest-Biogeosciences and Forestry* 9, 55-62.

346 Macfarlane, C., Hoffman, M., Eamus, D., Kerp, N., Higginson, S., McMurtrie, R., Adams, M., 2007.
347 Estimation of leaf area index in eucalypt forest using digital photography. *Agricultural and Forest*
348 *Meteorology* 143 (3–4), 176–188.

349 Möttus, M., Stenberg, P., & Rautiainen, M. (2007). Photon recollision probability in heterogeneous forest
350 canopies: Compatibility with a hybrid GO model. *Journal of Geophysical Research — Atmospheres*,
351 112, D103104. <http://dx.doi.org/10.1029/2006JD007445>.

352 Myneni, R.B., Knyazikhin, Y., Privette, J.L., Glassy, J., Tian, Y., Wang, Y., et al., 2002. Global products of
353 vegetation leaf area and fraction absorbed PAR from year one of MODIS data. *Remote Sensing of*
354 *Environment* 83, 214–231.

355 Nasahara, K.N., Muraoka, H., Nagai, S., Mikami, H., 2008. Vertical integration of leaf area index in a
356 Japanese deciduous broad-leaved forest. *Agricultural and Forest Meteorology* 148 (6–7), 1136–1146.

357 Nilson, T., 1971. A theoretical analysis of the frequency of gaps in plant stands. *Agricultural Meteorology*
358 8, 25–38.

359 Noormets, A., Gavazzi, M.J., McNulty, S.G., Domec, J.-C., Sun, G., King, J.S., Chen, J., 2010. Response of
360 carbon fluxes to drought in a coastal plain loblolly pine forest. *Global Change Biology* 16, 272–287.

361 Norman, J.M., 1982, Simulation of microclimates, in *Biometeorology in Integrated Pest Management*,
362 edited by J.L. Hatfield and I.J. Thomason, pp. 65–99, Academic, San Diego, Calif.

363 Piayda, A., Dubbert, M., Werner, C., Vaz Correia, A., Pereira, J.S., Cuntz, M., 2015. Influence of woody
364 tissue and leaf clumping on vertically resolved leaf area index and angular gap probability estimates.
365 *For. Ecol. Manage.* 340, 103–113.

366 Pisek, J., Chen, J. M., Lacaze, R., Sonnentag, O., Alikas, K., 2010. Expanding global mapping of the foliage
367 clumping index with multi-angular POLDER three measurements: Evaluation and topographic
368 compensation. *ISPRS Journal of Photogrammetry and Remote Sensing* 65, 341–346.

369 Pisek, J., Ryu, Y., Sprintsin, M., He, L., Oliphant, A.J., Korhonen, L., Kuusk, J., Kuusk, A., Bergstrom, R.,
370 Verrelst, J., 2013a. Retrieving vegetation clumping index from Multiangle Imaging SpectroRadiometer
371 (MISR) data at 275m resolution. *Remote Sens. Environ.* 138, 126–133.

372 Pisek, J., Sonnentag, O., Richardson, A., & Möttus, M., 2013b. Is the spherical leaf inclination angle
373 distribution a valid assumption for temperate and boreal broadleaf tree species. *Agricultural and*
374 *Forest Meteorology* 169, 186–194.

375 Pisek, J., Govind, A., Arndt, S.K., Hocking, D., Wardlaw, T.J., Fang, H., Matteucci, G., Longdoz, B., 2015.
376 Intercomparison of clumping index estimates from POLDER, MODIS, and MISR satellite data over
377 reference sites. *ISPRS J. Photogramm. Remote Sens.* 101, 47–56.

378 Pueschel, P., Buddenbaum, H., Hill, J., 2012. An efficient approach to standardizing the processing of
379 hemispherical images for the estimation of forest structural attributes. *Agric. For. Meteorol.* 160, 1–
380 13.

381 Qu, Y., Meng, J., Wan, H., Li, Y., 2016. Preliminary study on integrated wireless smart terminals for leaf
382 area index measurement. *Computers and Electronics in Agriculture* 129, 56–65.

383 Raabe, K., Pisek, J., Sonnentag, O., Annuk, K., 2015. Variations of leaf inclination angle distribution with
384 height over the growing season and light exposure for eight broadleaf tree species. *Agric. For.*
385 *Meteorol.* 214-215, 2–11.

386 Rambal, S., Ourcival, J.M., Joffre, R., Mouillot, F., Nouvellon, Y., Reichstein, M., Rocheteau, A., 2003.
387 Drought controls over conductance and assimilation of a Mediterranean evergreen ecosystem:
388 scaling from leaf to canopy. *Global Change Biology* 9, 1813–1824.

389 Rautiainen, M., Möttöus, M., Stenberg, P., 2009. On the relationship of canopy LAI and photon recollision
390 probability in boreal forests. *Remote Sensing of Environment* 113, 458–461.

391 Ross, J., 1981. *The Radiation Regime and Architecture of Plant Stands*. Junk Publishers,
392 The Hague, 391 pp.

393 Ryu, Y., Nilson, T., Kobayashi, H., Sonnentag, O., Law, B.E., Baldocchi, D.D., 2010. On the correct
394 estimation of effective leaf area index: Does it reveal information on clumping effects? *Agricultural*
395 *and Forest Meteorology* 150, 463–472.

396 Ryu, Y., Baldocchi, D.D., Kobayashi, H., Ingen, C., Li, J., Black, T.A., Beringer, J., Gorsel, E., Knohl, A., Law,
397 B.E., 2011. Integration of MODIS land and atmosphere products with a coupled- process model to
398 estimate gross primary productivity and evapotranspiration from 1 km to global scales. *Global*
399 *Biogeochemical Cycles* 25, GB40117.

400 Serbin, S. P., Gower, S. T., & Ahl, D. E., 2009. Canopy dynamics and phenology of a boreal black spruce
401 wildfire chronosequence. *Agricultural and Forest Meteorology* 149, 187–204.

402 Shabanov, et al., 2003. Effect of foliage spatial heterogeneity in the MODIS LAI and FPAR algorithm over
403 broadleaf forests. *Remote Sensing of Environment* 85, 410–423.

404 Sinclair, T.R., Murphy, C.E., Knoerr, K.R., 1976. Development and evaluation of simplified models for
405 simulating canopy photosynthesis and transpiration. *Journal of applied Ecology* 13, 813-829.

406 Smolander, S., Stenberg, P., 2005. Simple parameterizations of the radiation budget of uniform
407 broadleaved and coniferous canopies. *Remote Sensing of Environment* 94, 355–363.

408

409 Solberg, S., Brunner, A., Hanssen, K.H., Lange, H., Næsset, E., Rautiainen, M., Stenberg, P., 2009. Mapping
410 LAI in a Norway spruce forest using airborne laser scanning. *Remote Sens. Environ.* 113, 2317–2327.

411 Sonnentag, O., van der Kamp, G., Barr, A.G. and Chen, J.M., 2010. On the relationship between water
412 table depth and water vapor and carbon dioxide fluxes in a minerotrophic fen. *Global Change Biology*
413 16, 1762-1776.

414 Sprintsin, M., Cohen, S., Maseyk, K., Rotenberg, E., Grunzweig, J., Karnieli, A., et al., 2011. Long term and
415 seasonal courses of leaf area index in a semi-arid forest plantation. *Agricultural and Forest*
416 *Meteorology* 151, 565–574.

417 Stenberg, P., 2007. Simple analytical formula for calculating average photon recollision probability in
418 vegetation canopies. *Remote Sensing of Environment* 109, 221–224.

419 Stenberg, P., Kangas, T., Smolander, H., Linder, S., 1999. Shoot structure, canopy openness, and light
420 interception in Norway spruce. *Plant, Cell and Environment* 22, 1133–1142.

421 Stenberg, P., Palmroth, S., Bond, B., Sprugel, D., Smolander, H., 2001. Shoot structure and photosynthetic
422 efficiency along the light gradient in a Scots pine canopy. *Tree Physiology* 21, 805–814.

423 Stenberg, P., Möttus, M., Rautiainen, M., 2016. Photon recollision probability in modelling the radiation
424 regime of canopies—a review. *Remote Sensing of Environment* 183, 98–108.

425 Taugourdeau, S., le Maire, G., Avelino, J., Jones, J.R., Ramirez, L.G., Jara Quesada, M., ...Roupsard, O.,
426 2014. Leaf area index as an indicator of ecosystem services and management practices: an application
427 for coffee agroforestry. *Agriculture, Ecosystems and Environment* 192, 19–37.

428 Talbot, J., Roulet, N.T., Sonnentag, O., Moore, T.R., 2014. Increases in aboveground biomass and leaf area
429 85 years after drainage in a bog, *Botany* 92, 713-721.

430 Tanaka, N., Kume, T., Yoshifuji, N., Tanaka, K., Takizawa, H., Shiraki, K., Tantasirin, C., Tangtham, N.,
431 Suzuki, M., 2008. A review of evapotranspiration estimates from tropical forests in Thailand and
432 adjacent regions. *Agricultural and Forest Meteorology* 148, 807–819.

433 Tedeschi, V., Rey, A., Manca, G., Valentini, R., Jarvis, P.G., Borghetti, M., 2006. Soil respiration in a
434 Mediterranean oak forest at different developmental stages after coppicing. *Global Change Biology*
435 12, 110–121.

436 Thimonier, A., Sedivy, I., & Schleppei, P., 2010. Estimating leaf area index in different types of mature forest
437 stands in Switzerland: A comparison of methods. *European Journal of Forest Research* 129,543–562.

438 Urbanski, S., Barford, C., Wofsy, S., Kucharik, C., Pyle, E., Budney, J., McKain, K., Fitzjarrald, D., Czikowsky,
439 M., Munger, J.W., 2007. Factors controlling CO₂ exchange on timescales from hourly to decadal at
440 Harvard Forest. *Journal of Geophysical Research-Biogeosciences* 112 (G02020),
441 doi:10.1029/2006JG000293.

442 Verger, A., Martínez, B., Coca, F. C. D., & García-Haro, F. J., 2009. Accuracy assessment of fraction of
443 vegetation cover and leaf area index estimates from pragmatic methods in a cropland area.
444 *International Journal of Remote Sensing*, 30, 2685–2704.

445 Vuolo, F., Neugebauer, N., Bolognesi, S.F., Atzberger, C., D'Urso, G., 2013. Estimation of leaf area index
446 using DEIMOS-1 data: application and transferability of a semi-empirical relationship between two
447 agricultural areas. *Remote Sensing* 5, 1274–1291.

448 Wei, S., Fang, H., 2016. Estimation of canopy clumping index from MISR and MODIS sensors using the
449 normalized difference hotspot and darkspot (NDHD) method: The influence of BRDF models and solar
450 zenith angle. *Remote Sensing of Environment* 187, 476-491.

451 Yan, K., Park, T., Yan, G., Chen, C., Yang, B., Liu, Z., Nemani, R., Knyazikhin, Y., Myneni, R., 2016a.
452 Evaluation of MODIS LAI/FPAR product collection 6. Part 1: consistency and Improvements. *Remote*
453 *Sensing* 8, 359.

- 454 Yan, K., Park, T., Yan, G., Liu, Z., Yang, B., Chen, C., Nemani, R., Knyazikhin, Y., Myneni, R., 2016b.
- 455 Evaluation of MODIS LAI/FPAR product collection 6. Part 2: validation and intercomparison. Remote
- 456 Sensing 8, 460.

Figure 1
[Click here to download Figure: Pisek_2018_RSE_Fig1.pdf](#)

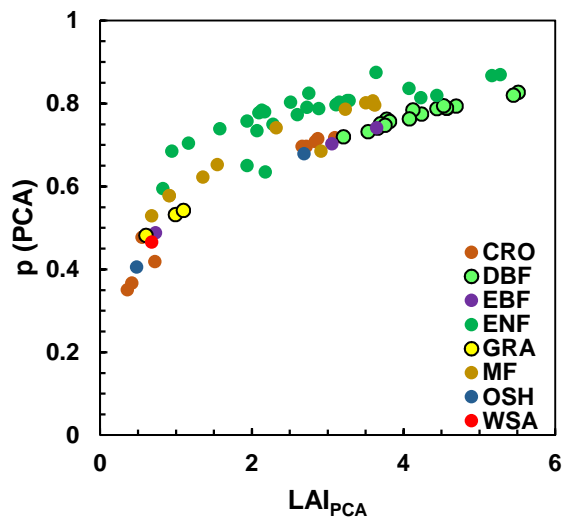


Figure 2

[Click here to download Figure: Pisek_2018_RSE_Fig2.pdf](#)

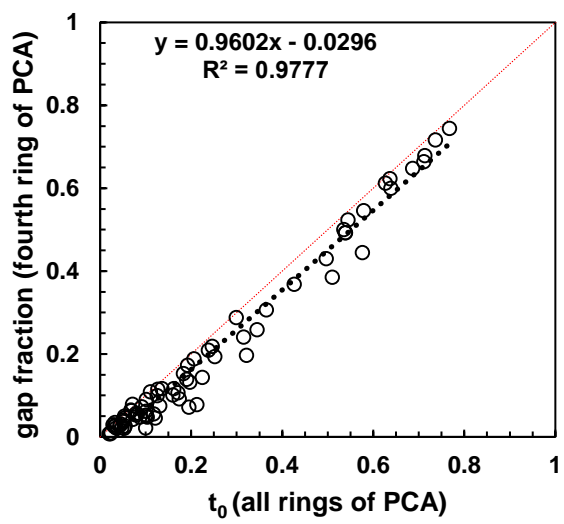


Figure 3AB

[Click here to download Figure: Pisek_2018_RSE_Fig3AB.pdf](#)

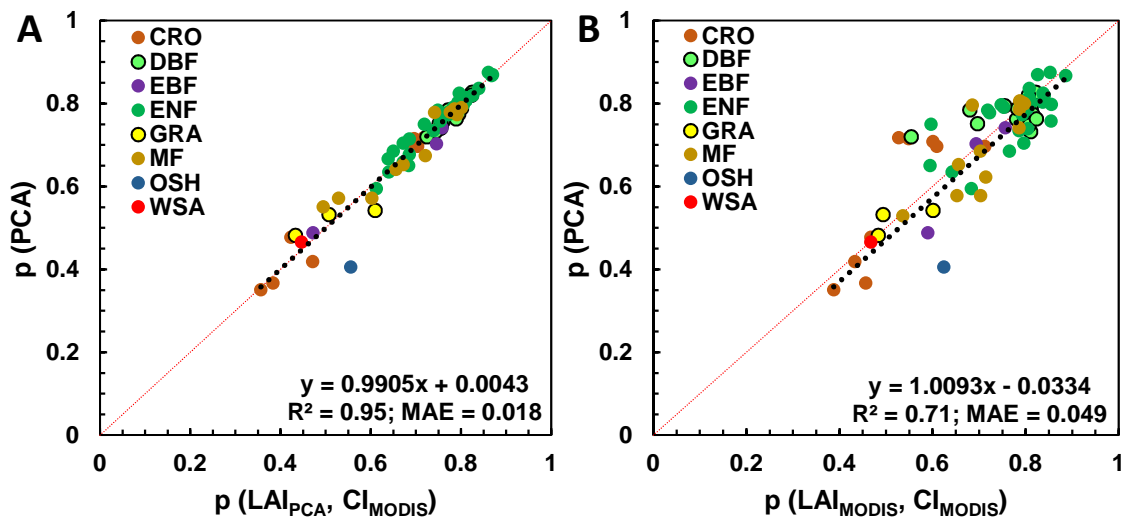


Figure 4

[Click here to download Figure: Pisek_2018_RSE_Fig4.pdf](#)

